博士論文 (要約)

Studies on function and structure of ferredoxin-dependent oxidoreductases from hyperthermophilic archaea

(超好熱性古細菌由来フェレドキシン依存性酸化還元酵素の機能と構造に関する研究)

氏名　閆　震

指導教員　伏信進矢

応用生命工学専攻

酵素学研究室

Contents

Chapter 1

General Introduction

1-1 Archaea and Hyperthermophiles

With the establishment of a novel phylogenetic tree on the basis of small-subunit rRNA (16S rRNA) sequence by Carl Woese (Fig 1-1), archaea have been increasingly known and studied as the third domain of organism, which are clearly distinguishable from domains of bacteria and eukarya [1-3]. Archaea form a unique and interesting group of organisms for the following reasons: First and foremost, archaea are critical for evolutionary studies to probe the origins of life and the course of evolution on earth because of their nearest location to the last universal common ancestor (LUCA) in the phylogenetic tree. Secondly, archaea are often recognizable as extremophiles, although not all extremephiles are members of the archaea (and not all archaea are extremophiles) [4]. Archaea are usually prevalent in extreme environments and hold some unique metabolic routes and unique enzymes [5]. As a result of their extremophilic nature and their role in the evolution of life, the properties of archaea have stimulated scientist to expand their horizons on many novel research [6-8].

Archaea have traditionally been grouped into methanogens, extreme halophiles (haloarchaea) and thermophiles. Hyperthermophiles, which grow fastest at temperature above 80℃ often colonize volcanic terrestrial environments and deep-sea hydrothermal vents, growing aerobically or anaerobically as heterotrophs or autotrophs [2, 9]. Actually, most hyperthermophiles exhibit a chemolithoautotrophic mode of nutrition. Molecular hydrogen, sulphide, sulphur and metal sulphides such as pyrite (FeS_2) can serves as electron donors. For anaerobic respiration, nitrate-, sulphate-, sulphur- and carbon dioxide (CO_2) can be used as electron acceptors, while for aerobic respiration, low concentration of oxygen can be used as electron acceptor [10, 11]. In most hyperthermophilic chemoautotrophes, CO_2 is the only carbon source required to build up organic cell material, and some novel assimilation ways of CO_2 into cellular components have also been discovered recently, for instance the hydroxypropionate-hydroxybutyrate cycle and dicarboxylate-hydroxybutyrate cycle (Fig

1-2).

The dicarboxylate-hydroxybutyrate cycle functions in the anaerobic or microaerobic autotrophic members of the crenarchaea orders, and can be divided into two parts: First, acetyl-CoA, CO_2 and bicarbonate are transformed into succinyl-CoA. Second, succinyl-CoA is converted into two molecules of acetyl-CoA. The hydroxypropionate-hydroxybutyrate cycle functions in the autotrophic crenarchaea order *Sulfolobus*. The enzymes of this cycle are oxygen tolerant, and the cycle can also be divided into two parts: The first transforms acetyl-CoA and two bicarbonate molecules to succinyl-CoA, and the second converts succinyl-CoA back into two acetyl-CoA molecules [12, 13]. In addition, several chemolithoautotrophic hyperthermophiles are opportunistic heterotrophs. Heterotrophic hyperthermophiles gain energy either by aerobic or different types of anaerobic respiration using organic material as electron donors, or by fermentation [10, 11].

1-2 Sulfolobus and Aeropyrum

Sulfolobus and *Aeropyrum* are two typical absolutely aerobic archaea. *Sulfolobus* species grow in volcanic springs with optimal growth occurring at pH 2-3 and temperature of 75-80℃. Generally, *Sulfolobus* either grow well chemoheterotrophically under aerobic conditions, but also can survive lithoautotrophically using sulfur to oxidize into sulfate [14, 15]. The principle metabolic pathways for heterotrophic growth are modified Entner-Doudoroff (ED) pathway (Fig 1-3) and tricarboxylic acid cycle (TCA cycle), which are linked by a pyruvate:ferredoxin oxidoreductase (PFOR) that catalyzes oxidative decarboxylation of pyruvate to produce acetyl-CoA. The modified ED pathway comprises a non-phosphorylative and a semi-phosphorylative branch[16, 17]. The complete genomes have also been sequenced for *Sulfolobus acidocaldarius* (2.23 Mbp), *Sulfolobus solfataricus* (2.99 Mbp), *Sulfolobus tokodaii* (2.69 Mbp) and nine species of *Sulfolobus islandicus* (2.4-2.8 Mbp) [18, 19]. However, approximately a half of open reading frame (ORF) are unknown function genes so far, and it is interesting and meaningful to study physiological functions and roles of these putative genes in the metabolism of *Sulfolobus* [20].

Aeropyrum pernix is the first strictly aerobic hyperthermophilic archaea growing at neutral pH. It was originally isolated from heated marine sediments and venting water in the sea off the coast of Japan. The optimal temperature for growth of *A. pernix* is 90-95℃, much higher than that of *Sulfolobus* [21]. Its complete genome (1.67 Mbp nucleotides) was sequenced in 1999, but there are still clearly a large amount of functionally unknown ORFs [22].

1-3 Ferredoxin

Ferredoxins (Fds) are distributed over a wide range of living organisms from humans to archaea. They are low molecular weight (6,000-12,000 Da), nonheme iron proteins that function as electron carriers in a wide variety of electron transport reactions. The name "ferredoxin", which literally means an iron redox protein with iron-sulfur cluster, composed of non-heme iron and acid labile sulfur. Various kinds of Fds isolated from different organisms have been studied biochemically and biophysically, and are classified by the geometry of Fe-S cluster into two types: the plant-type Fd and bacterial-type Fd [23-25].

Plant-type Fds are characterized not only by a single [2Fe-2S] cluster but also by an unique protein folding consisting of a four-stranded mixed β-sheet, an α-helix, and a long loop containing three of four cysteine ligands to the iron atoms [25]. Bacteria-type Fds have many variants which differ in the number of clusters (one or two), the type of cluster ([4Fe-4S] or [3Fe-4S]) and the length of polypeptide chain (insertion or terminal extension). The dicluster-type Fd, including two [4Fe-4S] clusters or [3Fe-4S] [4Fe-4S] clusters, have a common protein fold know as the (βαβ)2 fold, which ligates two cubane-like Fe-S clusters. Each of the duplicated halves of the common fold has the consensus amino-acid sequence, Cys-X-X-Cys-X-X-Cys-X-X-X-Cys-Pro, which is a striking feature for binding the Fe-S cluster [23, 24, 26].

Fd from *S. tokodaii* (StFd) is a bacterial dicluster-type. An 1.8 Å resolution crystal structure of StFd was determined by *Fujii, et al* (Fig 1-4). StFd is a unique zinc-ligating Fd with one [3Fe-4S] cluster and one [4Fe-4S] cluster [27]. Based on studies of electron paramagnetic resonance (EPR) and cyclic voltammetry, the [3Fe-4S] cluster with redox potential of -280 mV plays a redox role, whereas

the [4Fe-4S] cluster with redox potential of -530 mV plays a structural role [28]. The polypeptide chain of StFd consists of 103 amino-acid residues, and its primary structure is distinct from those of bacterial-type Fd in two regions: StFd has an N-terminal extension of 36 residues N-terminal domain and an insertion of about 10 residues in the middle of the polypeptide chain. Site-directed mutagenesis in the N-terminal domain including zinc-ligating His residues demonstrate that the zinc ion and a certain part of the N-terminal domain are responsible for thermal stabilization of the molecule, but not for function [29, 30].

1-4 2-Oxoacid:ferredoxin oxidoreductase (OFOR)

Oxidative decarboxylation of 2-oxoacids, such as pyruvate and ketoglutarate, is a key reaction of intermediary metabolism [31]. Most organism exploit the high reducing power of these substrates for the reduction of a low potential electron carrier and concomitant formation of an energy-rich thioester linkage between CoA and the resulting carboxylic acid. In mitochondria and many respiratory bacteria, the reactions are catalyzed by 2-oxoacid dehydrogenase (ODH) multienzyme complex, which is composed of three components, E1 (binding TPP), E2 (binding lipoamide), and E3 (binding flavins and final electron acceptor NAD^+), with a molecular mass of 5 – 6 MDa [32]. In archaea, early branching bacteria, and amitochondrial eukaryotes, the reactions are catalyzed by a much simpler enzyme, that is OFOR with subunit compositions of the a_2 type (homodimer), $(ab)_2$ type (dimmer of heterodimers), $(abcd)_2$ type (dimmer of heterotetramers) or other types, with maximum total molecular mass of around 270 kDa [33-36]. The thiamine diphosphate (TPP) and iron-sulfur cluster(s) are intrinsic cofactors. Fd is the external electron acceptor, which converted from oxidized state to reduced state (Fig 1-5). According to the type of 2-oxoacid, OFORs can be classified into the following four groups: pyruvate:ferredoxin oxidoreductase (PFOR), isovalerate:ferredoxin oxidoreductase (VFOR), ketoglutarate:ferredoxin oxidoreductase (KFOR) and indolepyruvate:ferredoxin oxidoreductase (IFOR).

OFORs from archaea such as *Pyrococcus furiosus*, *Archaeoglobus fulgidus*, *Methanococcus thermoautotrophilcum* as well as those from a pathogenic eubacterium, *Helicobacter pyroli*, are

composed of four different subunits, and are thus referred to as $(abcd)_2$ type enzymes [37-40]. Most of the enzymes of this type exhibit specificity for pyruvate. In certain organism, the coexistence of an enzyme specific for isovalerate has been reported (VFOR) [40, 41]. The OFORs from *S. tokodaii* (StOFOR) and *H. halobium* possess two different subunits of 71 kDa and 37 kDa [35, 42]. The a-Subunit is a homologue of a fusion of subunits c and a of $(abcd)_2$-type OFOR, in that order. StOFOR shows broad 2-oxoacid specificity not only for pyruvate, but also 2-oxobutyrate, ketoglutarate (KFOR), and so on, playing important roles in the central metabolism of glycolysis (or gluconeogenesis) and the TCA cycle. Another OFOR capable of acting on indolepyruvate (IFOR) has been found in *P. furiosus* and *P. kodakaraensis* KOD1, which are composed of two subunits [39, 43]. Subunit a is a chimera of subunits a, d and b of $(abcd)_2$-type OFOR, in that order. The OFORs specificity for pyruvate (PFOR) from *Klebsiella pneumoniae*, *Rhodospirillum rubrum*, *Enterobacter agglomerans*, *Anabaena variabilis*, *Trichomonas vaginalis* and *Desulfolvibrio africanus* are homodimers of a 120-130-kDa subunit, which is a fusion of subunits a, c, d and b, in that order [34, 44-47] (Table 1-1). Another novel PFOR from *Hydrogenobacter thermophilus* TK-6, which comprises five subunits (A, B, D, G, and E-subunits) is identified, and found that the A, B, G, E-subunits are similar to a, b, c, d subunits of $(abcd)_2$ type OFOR, respectively. D-subunit has no specific motifs but is essential for the enzyme expression [48]. Recently, this novel PFOR of five subunits was proved to act as pyruvate synthase catalyzing the reverse reaction to form pyruvate and play a critical role in the reductive tricarboxylic acid cycle of *H. thermophilus* TK-6 [49]. The molecular construction of the three types of OFOR, indicates that this family of enzymes should have evolved from a common ancestor, possibly of the $(abcd)_2$-type, through reorganization, deletion and fusion of the genes (Fig 1-6) [42].

Based on the structure of OFOR from *D. africanus* (DaPFOR), functional and structural analysis of a heterodimeric StOFOR has been carried out in our lab for long years. Although the two enzymes belong to the different types and show a low amino acid identity, they exhibit a certain level of domain similarities (Fig 1-7). The YPITP-motif (residues 253-257) in a-subunit, which is conserved universally in OFOR family, are essential for the turnover of the reaction rather than the affinity

toward 2-oxoacid [50]. In addition, based on careful multiple alignment of StOFOR and DaPFOR, five amino acids (T256, R344, T353 of a-subunit; K49, L123 of b-subunit) were selected as candidate 2-oxoacid recognizing residues. Replacement of the five residues resulted in significant changes in both of the K_m and V_{max} values for pyruvate, indicating that these amino acids are involved in substrate recognition and catalysis [51]. On the other hand, to elucidate the binding site for CoA in OFOR, an affinity labeling study of StOFOR using of 4-fluoro-7-nitrobenzofurazan (NBD-F), which mimic adenine ring of CoA, indicated that K125 in b-subunit is responsible for CoA binding [52]. Crystallization of StOFOR have also been carried out in our laboratory for long years, but the structure was not solved [Doctor thesis of Fukuda, and Master thesis of Maruyama and Osaki].

1-5 Ferredoxin:$NADP^+$ oxidoreductase (FNR)

Ferredoxin:$NADP^+$ oxidoreductases (FNRs) are ubiquitous FAD-containing enzymes that catalyze the electron transfer of reducing equivalents between Fd and $NADP^+$. In eukaryotes and eubacteria, FNRs can participate in electron transfer chains to oxidize reduced ferredoxin in various metabolic processes as diverse as photosynthesis, nitrogen fixation, steroid metabolism, oxidative-stress responses, iron sulfur cluster biogenesis, and so on [53, 54]. FNRs are generally classified into two types with four subclasses: the classical plant-type family comprising plastid and bacteria subclasses; and the glutathione reductase (GR) type family comprising adrenodoxin reductases (ARs) and oxygenase-coupled NADH-ferredoxin reductases (ONFRs). FNRs of the plant type function as a monomer. FNRs of the GR type are generally monomeric the exception being a homodimer of BphA4 from *Pseudomonas* sp. strain KKS102. Recently, a novel type of FNRs was reported, that is, thioredoxin reductase-like FNRs (TRLFs), which physiologically function as FNRs, but exhibit a structural homology to NADPH-dependent thioredoxin reductases (TrxRs). Other than the former two types, all known TRLFs are homodimers [55-57].

Although a large number of FNRs in different organisms have been characterized, and several FNR crystal structures have been solved, only one such enzyme in an archaea, called sulfide dehydrogenase, has been reported to show the activity of FNR from *Pyrococcus furiosus*. However, it

differs from the above three types of FNRs because not only is it a heterodimer of a subunit-a of 52 kDa and a subunit-b of 29 kDa, but also it contains a flavin and four iron-sulfur clusters. FNRs from other archaea have not been reported so far [58, 59].

1-6 The aim of this thesis

OFOR is a key enzyme in intermediate metabolism of many organisms including anaerobic bacteria, archaea and amitochondriate eukaryotes. In addition, OFOR are potential targets for specific drug design because they are only present in microgranisms that include several anaerobic human pathogens. Consequently, there has been an increased interest in the structure and catalytic mechanism of OFORs. But crystal structures of only one homodimeric type PFOR from *D. africanus* have been determined so far, and there are still a lot of unknowns on the reaction mechanism catalyzed by OFORs, such as electron transfer and substrate binding. The primary aim of this thesis is to solve the crystal structure of a $(ab)_2$-type OFOR, and reveal the reaction mechanism of oxidative decarboxylation of 2-oxoacid catalyzed by the simplest $(ab)_2$-type OFORs, which are not only TPP-containing enzymes, but also possess sole iron-sulfur cluster. These will provide a new insight and understanding for further studies in the classical key reaction.

On the other hand, it is still insufficient to elucidate the property and the physiological function of the Fds in *S. tokodaii*, and how the reduced StFd catalyzed by StOFOR recycles into its oxidized state remains unknown in hyperthermophilic aerobic archaea. Thus, this thesis also aims to further clarify the physiological functions of Fds in archaea. Moreover, I tried to find and characterize the archaeal FNRs which can recycle Fd in *S. tokodaii*.

Figures and Tables

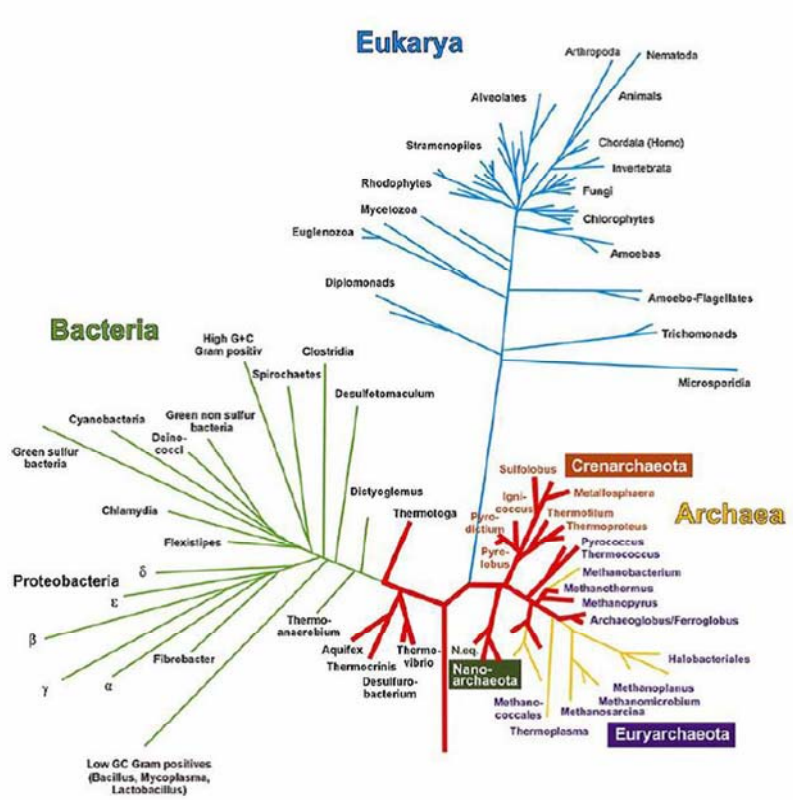

Fig.1-1. Universal phylogenetic tree based on small subunit rRNA. Red thick lines represent hypermophiles.

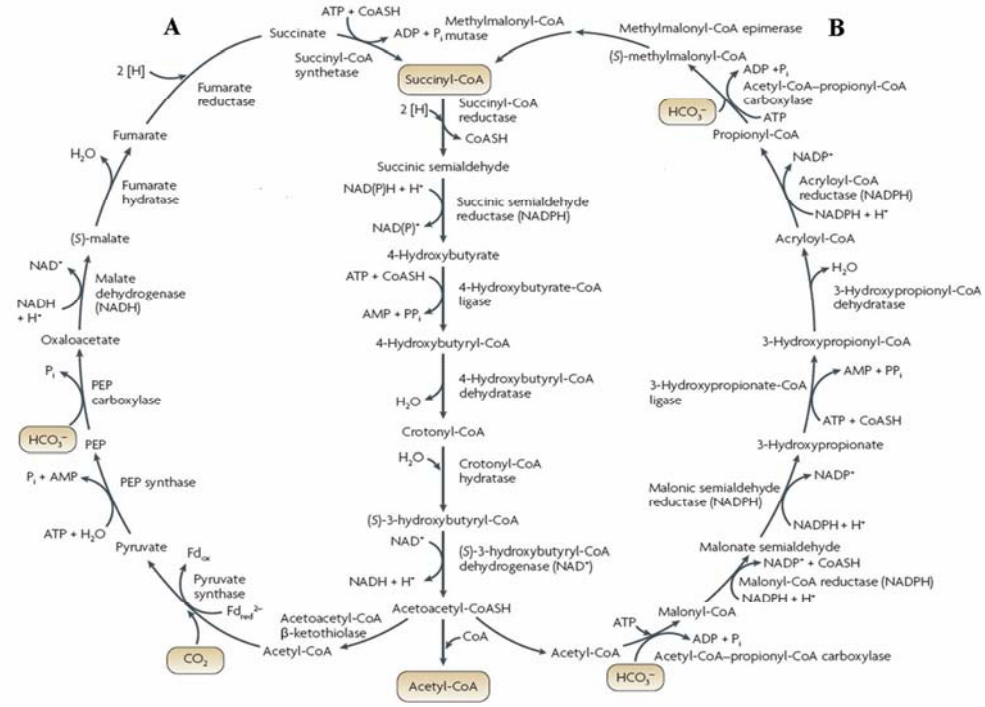

Fig.1-2. Pathways of autotrophic CO_2 fixation in crenarchaeota.

(A) The dicarboxylate-hydroxybutyrate cycle that functions in *Desulfurococcales* and *Thermoproteales*. (B) The hydroxypropionate-hydroxybutyrate cycle that functions in *Sulfolobus*.

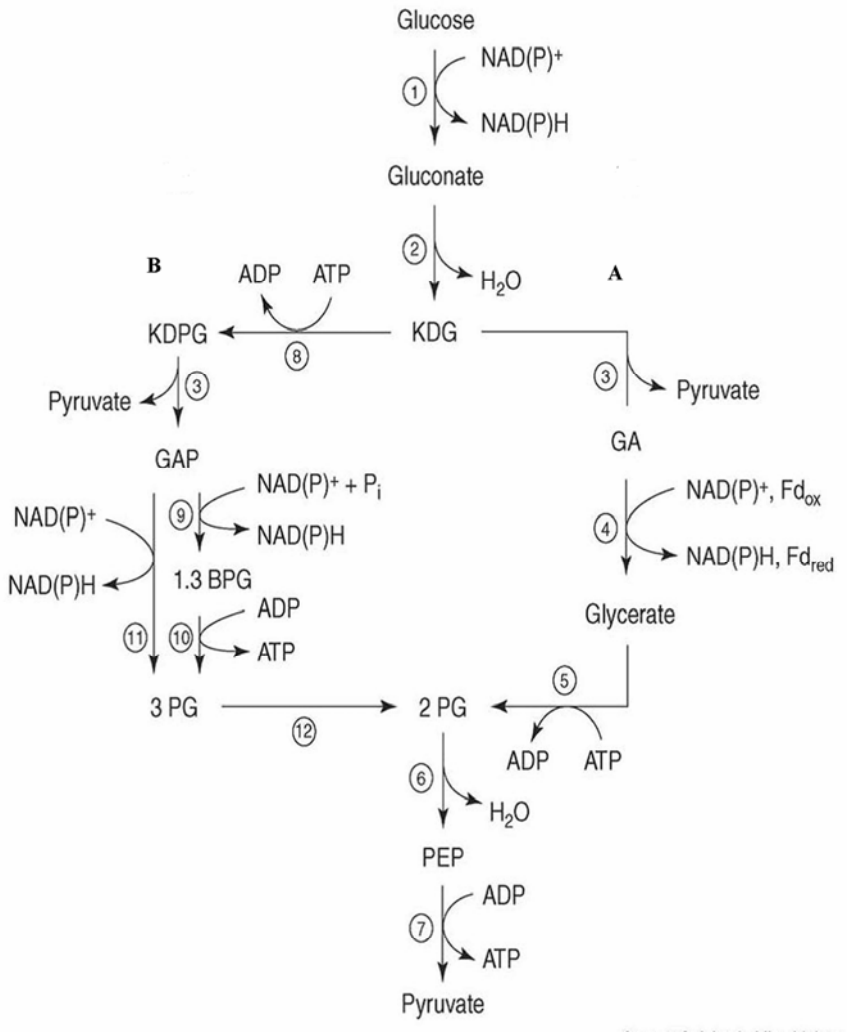

Fig.1-3. The Modified of the Entner-Doudoroff (ED) pathway in archaea. (A) Non-phosphorylative ED pathway. (B) Semi-phosphorylative ED pathway. Abbreviations: 1.3 BPG, 1,3-bisphosphoglycerate; Fd_{ox} and Fd_{red}, oxidized and reduced ferredoxin; GA, glyceraldehyde; GAP, glyceraldehyde-3 phosphate; KDG, 2-keto-3-deoxy-glucenate; KDPG, 2-keto-3-deoxy-6-phosphogluconate; PEP, phosphoenolpyruvate; 2 PG, 2-phosphoglycerate; 3 PG, 3-phosphoglycerate. Enzymes are numbered as follows: 1, glucose dehydrogenase; 2, gluconate dehydratase; 3, KDPG aldolase; 4, glyceraldehyde oxidoreductase; 5, glycerate kinase; 6, enolase; 7, pyruvate kinase; 8, KDG kinase; 9, glyceradehyde-3-phosphate dehydrogenase; 10, phosphoglycerate kinase; 11, non-phosphorylating glyceradehyde-3-phosphate dehydrogenase; 12, phosphoglycerate mutase.

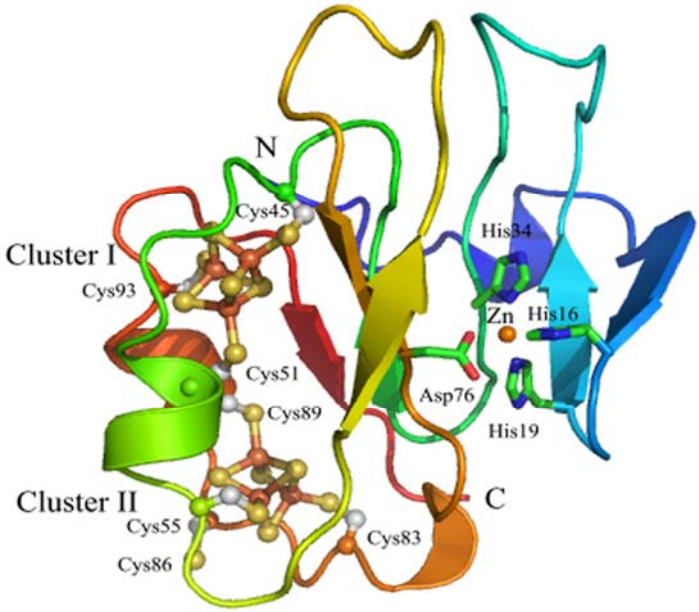

Fig.1-4. The crystal structure of ferredoxin from *Sulfolobus tokodaii* [27].

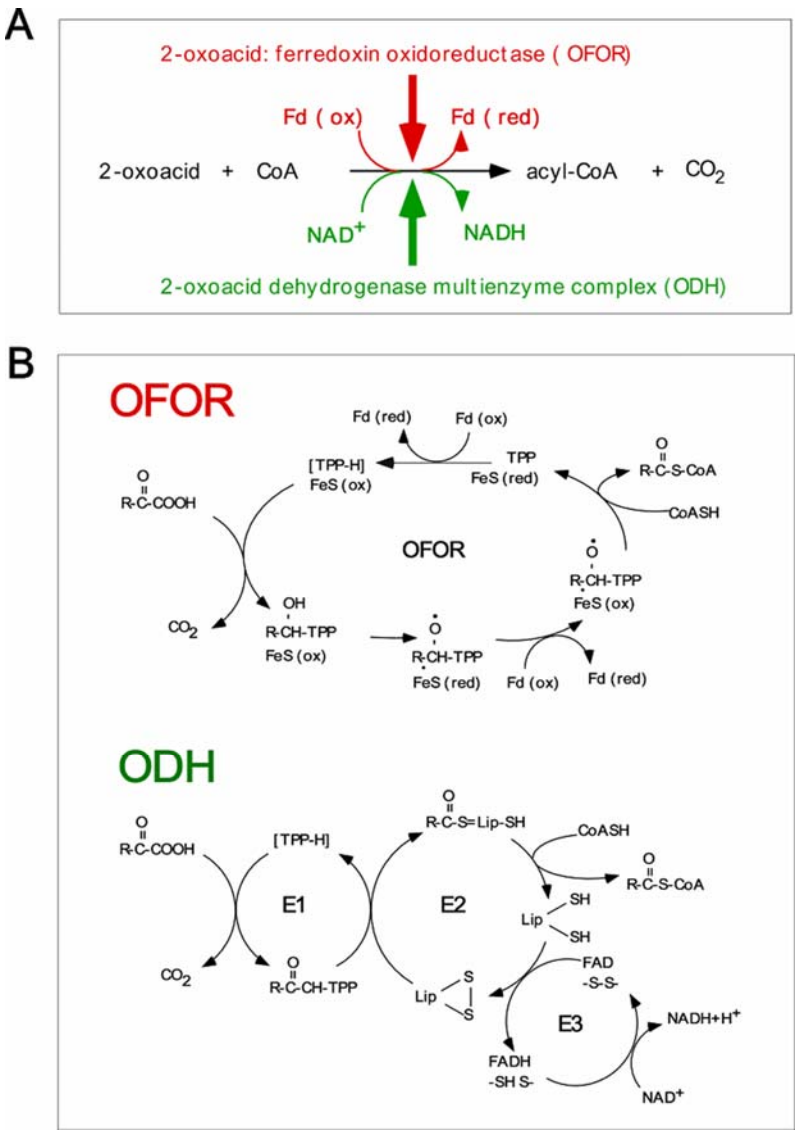

Fig.1-5. (A) The reaction catalyzed by OFOR and ODH multienzyme complex. (B) A comparison of reaction mechanisms catalyzed by OFOR and ODH. The OFOR reaction is shown only in the direction of oxidative decarboxylation during heterotrophic growth.

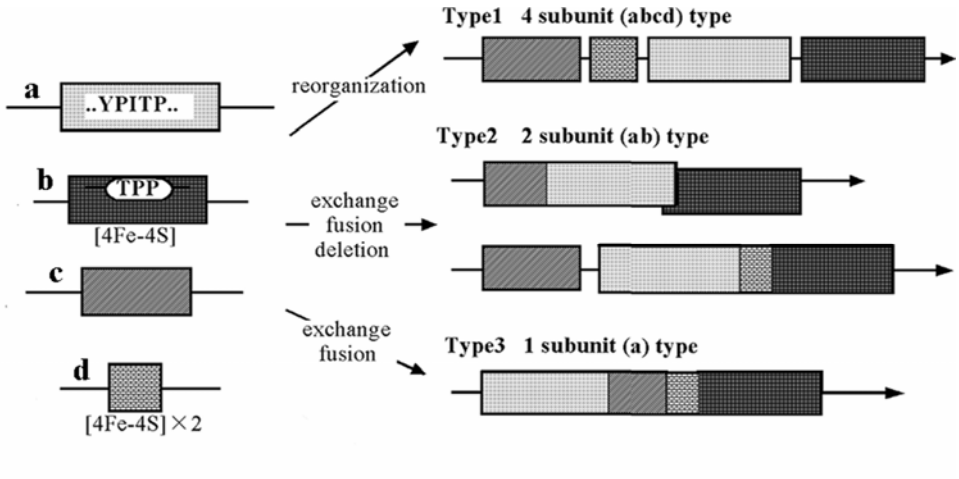

Fig.1-6. The molecular evolution of three types of OFORs

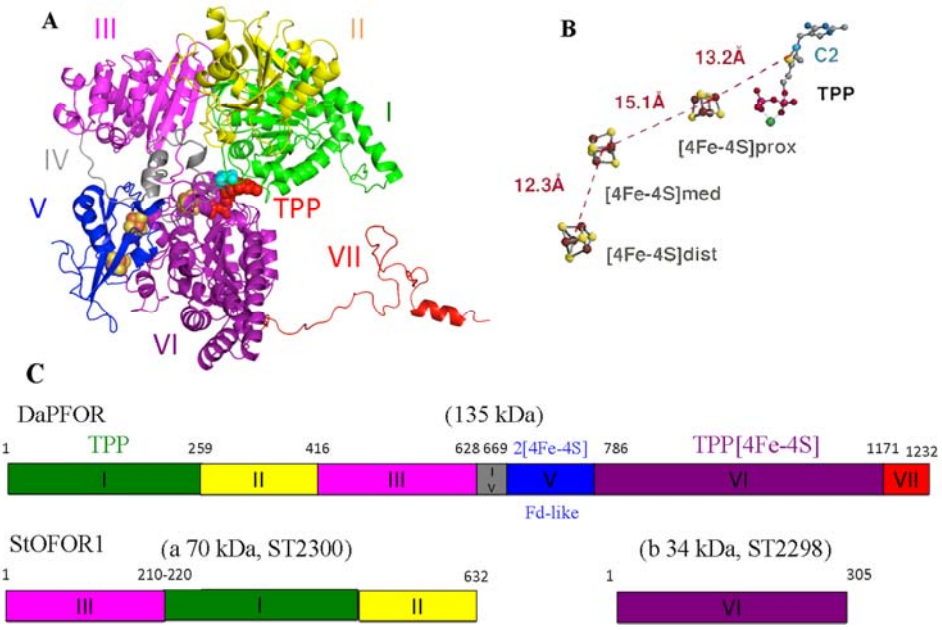

Fig.1-7. (A) The crystal structure of PFOR from *D. africanus* [60]. (B) Arrangement of TPP cofactor and three [4Fe-4S] clusters in one subunit, showing the successive center-to-center distances, assuming that the C2 atom is the redox center of TPP. (C) Domain similarities between StOFOR and PFOR from *D. africanus*.

Table.1-1. OFORs from various organisms.

Species	Enzyme	Total M.W. (K)	M.W. of the ssubunits a	b	c	d
Archea						
Sulfolobus tokodaii	OFOR	105	71	34		
Aeropyrum pernix K1	OFOR	115	69	36		
Aeropyrum pernix K1	OFOR	110	66	34		
Halobacterium salinarum	PFOR	256	86×2	42×2		
Pyrococcus furiosus	PFOR	155	44	30	20	12
P. furiosus	VFOR	155	44	35	20	12
P. furiosus	IFOR	180	66	23		
Thermococcus litoralis	VFOR	230	47	34	23	13
Archaeoglobus fulgidus	PFOR	116	45	33	25	13
Methanosarcina barkeri	PFOR	118	48	30	25	15
Methanobacterium thermoautotrophicum	PFOR	111	43	31	22	15
M. thermoautotrophicum	KFOR	107	40	31	24	12
M. thermoautotrophicum	IFOR	107	55	37	15	
M. thermoautotrophicum	VFOR	90	67	23		
Thermococcus kodakaraensis KOD1	IFOR	96	71	25		
Eubacteria						
Thermotoga maritima	PFOR	113	44	36	21	11
Hydrogenobacter thermophilus TK-6	PFOR	135	46	32	29	25
H. thermophilus TK-6	KFOR	105	70	35		
Helicobacter pylori	PFOR	121	47	36	24	14
Clostridium pasteurianum	PFOR	240	120×2			
Klebsiella pneumoniae	PFOR	240	120×2			
Rhodospirillum rubrum	PFOR	228	114×2			
Enterobacter aggromerans 333	PFOR		120			
Desulfovibrio africanus	PFOR		130×2			
Eucaryote						
Thrichomonas vaginalis	PFOR-A	240	123×2			
T. vaginalis	PFOR-B	240	123×2			
Entamoeba histolytica	PFOR	240	120×2			
Giardia	PFOR	240	123×2			

Chapter 2

Reaction mechanisms of 2-oxoacid:ferredoxin oxidoreductase from *Sulfolobus tokodaii*

2-1 Introduction

2-Oxoacid:ferredoxin oxidoreductases (OFOR), which are distributed among archaea, early branching bacteria, and amitochondrial eukaryotes, catalyzes CoA-dependent oxidative decarboxylation of 2-oxoacids such as pyruvate and ketoglutarate. According to the subunit compositions, OFORs are classified as the a_2 type (homodimer), $(ab)_2$ type (dimer of heterodimers), and $(abcd)_2$ type (dimer of heterotetramers). The TPP and iron-sulfur cluster(s) are intrinsic cofactors [31]. Homodimeric pyruvate:ferredoxin oxidoreductase from *Desulfovibrio africanus* (DaPFOR) is the only OFOR whose crystal structures have been determined (Fig 1-7) [60]. In a 135-kDa subunit, three [Fe-S] clusters are located between the TPP and the protein surface, providing an electron pathway from pyruvate to an external ferredoxin. The subunit is composed of seven domains; TPP binds between domains I and VI, one [4Fe-4S] cluster ("proximal") binds to domain VI, and two [4Fe-4S] clusters ("median" and "distal") bind to domain V (called intramolecular Fd) [61, 62]. OFOR from *S.tokodaii* (StOFOR) is $(ab)_2$ type, being composed of 70 kDa a-subunits (corresponding to a fusion of domains III-I-II of DaPFOR) and 34 kDa b-subunits (corresponding to domain VI of DaPFOR). Domain V of DaPFOR is lacking in StOFOR, that is, StOFOR contains only one [4Fe-4S] cluster, and is the simplest in the OFOR family (Fig 2-1). Therefore, this archaeal enzyme is a good model for studying the redox mechanism of OFOR [42, 50-52].

In a plausible model (Fig 2-2), the homodimeric type PFOR reaction starts from decarboxylation of pyruvate through attack by ylide of TPP, subsequently a hydroxyethyl-TPP (HE-TPP) intermediate being formed. From this intermediate an electron is transferred to the proximal [4Fe-4S] cluster and a radical of HE-TPP is formed. The radical is relatively stable, its half-life varying with the source of

PFOR from about a few minutes to more than several hours. The radical decays rapidly on the addition of CoA, an acceptor of a hydroxyethyl group, accompanied by transfer of another electron to the "medial" Fe-S cluster, producing acetyl- CoA and free TPP. For this reaction cycle to turnover, at least two intermolecular [4Fe-4S] clusters are required, since pyruvate releases two electrons while a [4Fe-4S] cluster usually transfers one electron immediately with a valence change between +2 and +1 [63-66]. Thus, PFOR cannot turnover in the absence of ferredoxin, which acts as an external electron sink [31, 67]. Therefore, whether or not a stable HE-TPP radical of StOFOR with a single [4Fe-4S] cluster in the absence of ferredoxin decays immediately on the addition of CoA is an interesting question. One of the purposes of the present study is to examine the reaction cycle of StOFOR with a single [4Fe-4S] cluster.

In addition to the classical oxidative decarboxylation reaction, OFOR can also catalyze non-oxidative decarboxylation of pyruvate to yield acetaldehyde, which is similar to that catalyzed by pyruvate decarboxylase, which contains TPP but not a Fe-S cluster. The archaeal OFOR reaction is so far assumed to require CoA for aldehyde production. The role of CoA remains unknown [68].

In this chapter, I constructed various mutants of StOFOR by replacing four Fe-ligating Cys residues with Ala, which yielded C12A, C15A, C46A, C197A, and C12/15A mutants, to investigate the roles of Cys residues in the reaction mechanisms of both oxidative and non-oxidative decarboxylation of pyruvate. We found that all four Cys are required to hold the [4Fe-4S] cluster for oxidative decarboxylation of pyruvate including the formation of a stable HE-TPP radical, and also found that CoA is not required for nonoxidative decarboxylation of pyruvate to yield acetaldehyde, thus proposed a revised reaction pathway for StOFOR.

2-2 Materials and Methods

2-2-1 Plasimid and Bacterial strains

An expression plasmid, pPKORCHis, with a His tag at the C-terminal of b-subunit was constructed from the original plasmid, pOFORAB [50-52]. Genes encoding the a-subunit and b-subunit of OFOR were amplified by PCR reaction from pOFORAB. Primers pkorANhe-If and

pkorBXho-Ir-stop were designed as follows: 5'-ATATGGCTAGCAGACTTAGTTGGGTTATAGG-3' and 5'-GATCTGCTCGAGTTAGTCTACTTCCCTTTCTTTTA-3', and the PCR product was ligated into an expression vector, pET-21a, between the Nhe I and Xho I sites. *E.coli* strain XL10 gold was used for cloning of the wild type and mutant OFORs. *E.coli* strain C43 (DE3) was used for protein expression of the wild type and mutants.

2-2-2 Construction of mutant plasimid

Site-directed mutagenesis of C197A, C46A, C12A, C15A, and C12/15A was performed according to the PrimeSTAR site-directed mutagenesis protocol (TaKaRa) with the following primers: 5'-CAACCTGCCCCTACTTACAACGATATA-3', 5'-ATTGGTGCCTCTGGTAAAATACCGCAT-3', 5'-GTGCCCTGGAGCCGGTAATTTCGGAATTTTA-3',
5'-GGCCCCTGGATGCGGTAATTTCGGAATTTTA-3',
5'-GGCCCCTGGAGCCGGTAATTTCGGAATTTTA-3'. The sequences were confirmed by the dideoxy chain termination method with an Applied Biosystems Model 373A DNA sequencer.

2-2-3 Heterologous expression and purification of wild type and mutant OFOR

Cells harboring the expression plasmid for the wild type and mutant OFOR genes were grown in LB-ampicillin (100 μg/ml) medium until OD_{600} reached 0.8-1.0 at 37℃. Then 0.5 mM β-isopropylthiogalactoside (IPTG) was added and the cells were grown for a further 20 h at 30℃. The cells were then collected and suspended in 50 mM Tris-HCl buffer, pH 8.0, and disrupted by sonication. The lyzed cell suspension was heated at 70℃ for 15 min to denature *E.coli* proteins. After centrifugation of the mixture to remove denatured proteins, the supernatant was subjected to Ni affinity chromatography on a HisTrap FF crude 5 ml column. The column was washed with 50 mM Tris-HCl buffer, pH 7.5, and then the proteins eluted with 50 mM Tris-HCl, 500 mM imidazole buffer, pH 7.5, were collected. Afterwards, the sample was subjected to Superdex-200 column chromatography with equilibration with 20 mM Tris-HCl 250mM NaCl buffer, pH 7.5. The sample was eluted as main peak monitored by A_{280} as purified StOFOR.

2-2-4 Assay methods for enzyme activities

Oxidative decarboxylation activity was assayed by two methods. One is based on

pyruvate-dependent reduction of methylviologen monitored at A_{578} and 80℃, as described previously [50-52]. The standard assay mixture (0.4 mL) comprised 50 mM Tris-HCl buffer, pH 8.5, 10 mM pyruvate, 0.25 mM CoA, 2 mM methylviologen, and the wild type or a mutant OFOR. The other method is Fd-dependent reduction of horse heart cytochrome *c* monitored at A_{550} and 50℃ using *Sulfolobus* 7Fe ferredoxin purified as reported. The standard assay mixture (0.4 mL) comprised 20 mM potassium phosphate buffer, pH 7.0, 10 mM pyruvate, 0.25 mM CoA, 50 μM horse heart cytochrome c, 20 μM *Sulfolobus* 7Fe ferredoxin, and the wild type or a mutant OFOR [42].

Acetaldehyde production activity was measured as follows: for the routine assay [68], a 0.4 ml mixture was prepared in a 1.5 ml microcentrifuge tube and contained the following: 50 mM Tris-HCl buffer, pH 8.5, 10 mM pyruvate, 0.5 mM CoA, and 40 μg wild type or mutant OFOR. The tube was shaken in a water bath at 80℃ for different times, and the reaction was stopped by cooling on ice bath. To estimate acetaldehyde production, the above reaction mixture was transferred to a cuvette and incubated with 0.2 mM NADPH at 50℃ for 1 min, and then A_{340} was recorded before and after the further addition of 2 U of alcohol dehydrogenase [69] from *Thermoanaerobium brockii* (Sigma). The difference in A_{340} was used for calculation of acetaldehyde production, using ε_{340} = 6.2 mM/cm.

2-2-5 Optical spectral analyses and Fe content

Absorption spectra were recorded with a JASCO V-560 spectrophotometer. The Fe content was determined with an inductively coupled plasma atomic emission spectrometer SPS3500 and also a Z-9000 simultaneous multi-element atomic absorption spectrophotometer. Standard solutions of Fe were purchased from Wako Pure Chemicals. The protein samples (200 μg) were oxidatively hydrolyzed at 90℃ in HNO_3 overnight and then dissolved at a concentration of 0.2 mg protein/ml in 0.1 N nitric acid.

2-2-6 Circular dichroism (CD) measurements

CD spectra were recorded with a JASCO J820 spectropolarimeter using drum cells of 0.1 and 1 cm light paths at room temperature (25˚C). The protein concentrations were 0.1 mg/ml and 0.5 mg/ml in 5 mM Tris-Cl, pH 7.5, for the far UV region (190-260 nm) and near UV-visible region (260-550 nm),

respectively. The averages of eight scans are shown as molar ellipticity using the residue number of 932 and molecular weight of 104k.

2-2-7 EPR measurements

EPR spectra were measured with a JES-FA100 spectrometer. The measurement temperature was controlled with a JEOL ES-CT470 cryostat system and a digital temperature controller model 9650. The magnetic field was calibrated with a JEOL NMR field meter ES-FC5. The g-values was determined by spectral simulation using JEOL ANISIMU/FA software, version 2.0.0.

2-2-8 Cyclic voltammetry

Electrochemical measurements were carried out with an Omni101 microprocessor- controlled potentiostat (Cypress Systems Inc.) using a pyrolytic graphite electrode (BAS). The counter electrode was a platinum wire and the reference electrode was a Ag/AgCl/3M KCl electrode (210 mV vs NHE). The sample solution comprised 0.1 mM enzyme, 100 mM NaCl, and 2 mM tobramycin in 5 mM TrisCl, pH 7.5, with argon gas flow maintained during the experiment at 25˚C.

2-3 Results

2-3-1 Selection of four residues that bind with an FeS cluster

The only reported three-dimensional structure of an OFOR family member is that of DaPFOR, which is composed of seven domains [60, 62]. TPP binds at the interface of domains I and VI, and an atypical [4Fe-4S] cluster, which binds to domain VI, is ‘proximal’ to the diphosphate group of TPP (Fig 1-7). The other two clusters, called the ‘median’ ones and ‘distal’ according to their distance from the TPP cofactor, are contained in ferredoxin-like domain V. Whereas, StOFOR has only one [4Fe-4S] cluster ligated by four Cys residues in subunit b [42], which is supposed to align with domain VI of the DaPFOR. Four Cys residues in domain VI of DaPFOR contribute to the [4Fe-4S] cluster binding: Cys812, Cys815, Cys840, and Cys1071, which correspond to Cys12, Cys15, Cys46, and Cys197 in subunit b of StOFOR, respectively. No other Cys residue is present in StOFOR. Therefore, we constructed various mutants of StOFOR with the Fe-ligating Cys residues replaced with Ala, the mutants being named C12A, C15A, C46A, C197A, and C12/15A, respectively.

2-3-2 Expression and purification of wild type and mutant OFORs

Mutant OFORs were constructed by means of the PrimeStar site-directed mutagenesis method (TaKaRa) according to the protocol recommended by the manufacturer. The expression and purification were conducted as described under Materials and methods. Purified samples gave two main bands for a-subunit (70kDa) and b-subunit (35kDa) on SDS-PAGE (Fig. 2-3).

2-3-3 Metal contents of purified StOFORs

Fe-contents were determined by ICP-AES and an atomic absorption spectrophotometer as described under Materials and methods. The two methods showed strikingly similar Fe contents (99±1 ppb, 38.7±0.7 ppb, 22.2±0.2 ppb, 7.7±0.3 ppb, 10±2 ppb, and 6.5±0.5 ppb) for the wild type (0.075 mg/ml), C197A (0.07 mg/ml), C46A (0.07 mg/ml), C15A (0.066 mg/ml), C12A (0.073 mg/ml), and C12/15A (0.064 mg/ml), respectively. The purified enzyme contained 2.77 mol of non-heme Fe per 1 mol of wild type StOFOR, this value being almost the same as that previously reported [42]. The value is probably an underestimate due to overestimation of the protein amount, as often experienced for other FeS proteins [28, 39, 41, 70]. The results are in good agreement with one [4Fe-4S] cluster per StOFOR, as deduced from the amino acid sequence. The mutant StOFORs, C197A, C46A, C15A, C12A, C12/15A, respectively, contained 1.11, 0.62, 0.23, 0.24, and 0.19 mol non-heme Fe/mol protein. These results indicate that replacement of Cys 197, 46, 15, or 12, or both Cys 15 and 12 with Ala caused the destruction of the [4Fe-4S] cluster. In particular, the Fe content of C197A is apparently higher than other mutants.

2-3-4 Spectroscopic properties of wild type and mutant StOFORs

Fig. 2-4 shows the absorption spectra of the wild type and all mutant OFORs. The UV-visible absorption spectra of the wild type OFOR showed a peak at 280 nm and a broad shoulder around 410 nm, characteristic of FeS proteins [31, 42]. The absorbance ratios of A_{410}/A_{280} were 100%, 59.7%, 37.5%, 28.4%, 30.7%, and 11.5% for the wild type, C197A, C46A, C15A, C12A, and C12/15A, respectively. A_{410} was decreased by 40-70% for single Cys mutants, and by almost 90% for double mutant C12/15A. C197A showed about 60% of A_{410} compared to the wild type.

Upon the addition of pyruvate to the enzyme, the formation of a 320-nm chromophore was

detected for the wild type StOFOR (Fig. 2-5A, trace 4). This is in agreement with the previous reports on StOFOR, and the PFORs from *M. barkeri* and *D. africanus* [34, 71]. Further addition of CoA leads to partial bleaching of the 320-nm chromophore, as well as a decrease in the absorbance between 380 and 480 nm, which corresponds to reduction of the iron-sulfur cluster (Fig. 2-5A, trace 5). In contrast, formation of the 320-nm chromophore was not observed upon addition of pyruvate to any of the mutant StOFORs. Further addition of CoA caused no change in the spectrum (traces 4 and 5 in Fig. 2-5 B and C).

The wild type StOFOR showed low-intensity EPR signal ($g_{//}$ = 2.03, $g_{\perp}$ = 2.01) attributed to the oxidized state of S = 1/2 $[4Fe\text{-}4S]^{2+}$ cluster (Fig. 2-6 A, trace 1), similar to that of the reported PFOR [35, 71], a transcription factor fumarate nitrate reductase of *E. coli*, and aconitase from *Sulfolobus acidocaldarius*, which possess a single $[4Fe\text{-}4S]^{2+}$ cluster under anaerobic condition [72, 73]. The EPR signal of these proteins under aerobic conditions are reported to be $[3Fe\text{-}4S]^{2+}$ derived from deletion of single Fe atom from the $[4Fe\text{-}4S]^{2+}$ cluster through oxidative damage [70, 71]. When the enzyme was mixed with pyruvate, there was an intense EPR signal centered at g = 2.00 (Fig. 2-6 A, trace 2), previously reported to result from TPP-based free radical intermediate. After overnight incubation of the enzyme with pyruvate, the EPR signal was unchanged. Upon further addition of CoA, the signal of the HE-TPP radical immediately markedly decreased, indicating the decay of the radical intermediate (Fig. 2-6 A, trace 3). The results are consistent with those observed for other OFORs [34, 35, 65, 71]. In contrast to the wild type OFOR, the intense signal of a radical intermediate was not observed at all for any of the mutant StOFORs, including C197A (Fig. 2-6 B-D). Therefore, we suggest that the special 320-nm chromophore observed for the wild type OFOR represents the HE-TPP radical intermediate.

The mutant C197A unexpectedly showed a high-intensity EPR signal, which shares similar g-value with the [3Fe-4S] cluster as shown above. Taking the high Fe content (>1 mol per mole) enzyme into account, some kind of iron-sulfur cluster, possibly partially decomposed product of [3Fe-4S] cluster, may be held in the protein, since C197A showed low activity of oxidative

decarboxylation compared to wild type. Other mutants were almost EPR silent (Fig. 2-6 B-D). Taking the low Fe content (<1 mol per mole) of mutant enzymes into account, these mutants lack an iron-sulfur cluster. Throughout the magnetic field, a $g = 4.3$ signal was not observed for any mutant (Fig. 2-6 E), suggesting that neither a rubredoxin type cluster or ferrous ion was included in the sample.

The CD spectra of the wild type StOFOR, C197A, and C12/15A are shown in Fig. 2-7. In the far UV region, similar spectra were observed for these enzymes (Fig. 2-7 A) indicating that the secondary structure or main-chain folding is almost the same in them, although a slight decrease in the depth of the trough at 222 nm for C197A and C12/15A, and a slight decrease in the height of 195 nm peak for C12/15A are noticable, while in the near UV-visible region (Fig. 2-7 B), wild type enzyme showed a sharp peak at 292 nm and a broad trough around 325 nm, which are observed for a number of TPP-dependent enzymes and its detection strongly depends on pH and enzyme environment [74]. Wild type StOFOR showed a broad peak and trough at 360 nm and a broad trough at 450 nm, which were also observed in other [4Fe-4S] cluster protein [75, 76], but not in C197A and C12/15A.

2-3-5 Redox potential and charge

On cyclic voltammetry (Fig. 2-8), the wild type StOFOR showed two redox couples corresponding to redox potentials of -545 mV and 176 mV, that of C197A being 195 mV. The redox potential of [3Fe-4S] ferredoxin from *Desulfovibrio gigas* is reported to be -130 mV vs NHE [77]. The values 176 mV and 195 mV are much higher, which may be artifacts at the electrode surface and not physiological. The redox potential of -545 mV for the wild type StOFOR is similar to the value (-540 mV) reported for the proximal [4Fe-4S] cluster in DaPFOR [65], suggesting that the single [4Fe-4S] cluster in StOFOR physiologically switches between 2+ and 1+ under physiological conditions. No redox potential were observed in the C12/15A, whose iron-sulfur cluster is completely destructed.

On Native-PAGE (Fig. 2-9), the bands of wild type, C197A and C12/15A migrate in different rates (in the reverse order) from negative to positive direction, which may be related to the electric charge of the cluster, for instance, +2, +1 and 0, respectively.

2-3-6 Ability of oxidative decarboxylation of pyruvate

The ability of oxidative decarboxylation was assayed by two methods using (A) the artificial electron acceptor methylviologen at 80℃ or (B) Fd-dependent reduction of horse heart cytochrome *c* at 50℃. The results are summarized in Table 2-1. The relative specific activities of the wild type, C197A, C46A, C12A, C15A, and C12/15A enzymes were 100%, 8%, 2.2%, 1.9%, 0.8%, and 0.33% in assay A, and 100%, 45.9%, 8.1%, 5.4%, 3.8%, and 1.1% in the assay B, respectively. The specific activities of the enzyme, 3.64 U/mg at 80℃ in assay A, and 0.37 U/mg at 50℃ in the assay B almost follow the temperature dependence of the reaction.

A comprehensive analysis of the integrity of the FeS cluster and the specific activities of all kinds of OFORs suggest that an intact [4Fe-4S] cluster is essential for full activity. Even when a single Cys was replaced, the FeS cluster was almost completely destroyed and the enzyme activity decreased to less than 3% of that of the wild type enzyme, with the exception of the C197A mutant, which showed a high intensity EPR signal resembling that of the [3Fe-4S] cluster, but only showed about 8% activity in assay A and 46% in assay B compared to the wild type. When two Cys were replaced, the enzyme lost most of the activity as well as the FeS cluster.

2-3-7 Ability of non-oxidative decarboxylation of pyruvate

StOFOR produced acetaldehyde from pyruvate in the absence of an electron acceptor (Fig. 2-10). Such non-oxidative decarboxylation has been reported for *P. furiosus* OFOR, which is totally dependent on CoA [68]. In contrast, CoA was not essentially required for StOFOR. It enhanced the activity by about 20 % (Table 2-2). The specific activities of the wild type and mutant OFORs were calculated from the initial velocity to be 0.051 – 0.077 μmol/min/mg at 80˚C (Table 2-2). *P. furiosus* PFOR shows similar velocity of acetaldehyde formation [68]. These values are about 2 % of the rate of oxidative decarboxylation of StOFOR. Similar specific activity was found to be catalyzed by wide type as well as mutants lacking the intact [4Fe-4S] cluster. Even in the absence of CoA, about 80% of the activities was observed. This suggests that the intact FeS cluster is not responsible for non-oxidative decarboxylation of pyruvate yielding acetaldehyde. The remarkable point is that neither

CoA nor anaerobic conditions were required for the acetaldehyde-forming activity of StOFOR.

2-4 Discussion

StOFOR is the simplest OFOR and serves as a good model for investigating the reaction mechanism, because of not only simple domain composition but also the existence of only one [4Fe-4S] cluster. Taking advantage of this, we constructed various mutants by replacing the four Fe-ligating Cys residues with Ala.

As a result, we found that all the mutants lost the [4Fe-4S] cluster as well as most of the oxidative decarboxylation activity. C197A held some incomplete iron-sulfur cluster, which is not attributed to typical [3Fe-4S], [2Fe-2S], nor a unique cysteine-persulfide-ligated [2Fe-2S] cluster [72, 78, 79]. The sulfur-atom of Cys197 is deduced to be located furthest from the active site thiazole ring compared to other cysteinyl sulfur atom, and its replacement with Ala may immediately allow the release of ligating Fe atom, followed by successive degradation into unidentified state. The questions remain as to why C197A is different from the other mutants, and why the four residues of Cys exert a different effect in holding the [4Fe-4S] cluster. Through comparison with the proximal [4Fe-4S] cluster of DaPFOR, we found that Cys1071 in DaPFOR (Cys197 in StPFOR) is located furthest in the [4Fe-4S] cluster from the thiazole ring of TPP compared to the other three Cys (812, 815, and 840). Furthermore, Cys197 in StOFOR is located between two Pro residues (Pro196 and Pro198), which may restrict the position of Cys197, even when replaced with Ala, making the effect of mutation on the main chain much smaller than in the case of others.

In the oxidative decarboxylation reaction of StOFOR, the hydroxyethyl-TPP (HE-TPP) radical intermediate is detected not only as an EPR signal but also as a 320 nm-chromophore, as reported for the PFORs from *M. barkeri* [71] and *D. africanus* [34]. In certain cases, radical decay is followed by a decrease in the absorbance at around 400 nm which represents the S-to-Fe charge [64].

The stability of the HE-TPP radical intermediate depends on the source of OFOR. In contrast to PFOR from *Moorella thermoacetica* with a half-life of approximately 2 min [65], a much stable

radical is formed for archaeal OFOR [31]; OFOR from *S. tokodaii* shows that for more than a day at room temperature (data not shown). But on the addition of CoA, the rate of radical decay increased for every OFOR, and in the case of *M. thermacetica*, a 100 000-fold increase was observed [64].

For StOFOR, the radical was relatively stable, there being no decay even after incubation at room temperature overnight (data not shown). Rapid radical decay on the addition of CoA was observed for StOFOR, which was completed within a few minutes at room temperature. In contrast to other PFORs with three iron-sulfur clusters, the reduced $[4Fe\text{-}4S]^{1+}$ in StOFOR cannot be reconverted into $[4Fe\text{-}4S]^{2+}$ without electron efflux to external ferredoxin. In the absence of ferredoxin, CoA added to the HE-TPP radical was not acetylated and appeared to remain unchanged, and the reaction seemed to proceed toward non-oxidative decarboxylation yielding acetaldehyde with a single turnover. CoA acts on the TPP radical and converts it into acetyl CoA in the presence of ferredoxin, or possibly into acetaldehyde in the absence of ferredoxin.

An additional function of various PFORs is CoA-dependent non-oxidative decarboxylation yielding acetaldehyde [68]. With regard to *P. furiosus* PFOR, CoA plays a structural rather than a catalytic role, and ferredoxin is not necessary. In contrast, the wild type StOFOR and all the mutants showed similar non-oxidative decarboxylation activity producing acetaldehyde, even without CoA, which is completely the same as the reaction catalyzed by pyruvate decarboxylase (PDC) [80]. This finding demonstrate that the TPP active site is operational and fully functional, irrespective of whether the FeS cluster is correctly formed or not [81].

Based on all of the data regarding the kinetic and redox center of StOFOR, a “switch” mechanism for the dual activity of this enzyme [68] was revised, as shown in Fig 2-11. The reaction starts with nucleophilic attack by the ylid form of TPP on the carbonyl carbon of pyruvate (step 1), and after the release of CO_2, a hydroxyethyl-TPP (HE-TPP) intermediate is generated (step 2). The conversion of the HE-TPP intermediate in to either acetyl-CoA or acetaldehyde depends on the completeness of the FeS cluster in the redox center of the OFOR and the existence or not of ferredoxin. When the first electron is transferred from HE-TPP to the $[4Fe\text{-}4S]^{2+}$ cluster, a HE-TPP radical intermediate is

generated (step 3), and external ferredoxin approaches the OFOR to oxidize the reduced [4Fe-4S] cluster from +1 to +2. The next step involves the binding of CoA to the HE-TPP radical intermediate, and another electron is transferred from the HE-TPP radical to $[4Fe\text{-}4S]^{2+}$ (step 4), which has been re-oxidized through the release of an electron to external ferredoxin. The oxidative decarboxylation is completed and acetyl-CoA is released (step 5). To turnover the reaction cycle of the enzyme, external ferredoxin is supposed to oxidize the reduced [4Fe-4S] twice from +1 to +2. Under the conditions without ferredoxin, steps 6 – 8 may proceed as deduced from the EPR experiments. After formation of the HE-TPP radical (step 6), binding with CoA leads to rapid decay of the HE-TPP radical (steps 7 - 8), but the mechanism of CoA binding with the HE-TPP radical and the fate of CoA remains to be elucidated. Three possible mechanisms for CoA binding with the HE-TPP radical intermediate have been proposed by Ragsdale in the case of an OFOR with three clusters [64]. All of the three mechanisms seem not to be applicable to StOFOR with only one cluster since the second cluster must be reduced accompanied by CoA binding. However, one of the mechanisms was further modified by Tittmann, that is, the formation of a low potential (highly reducing) anion radical through nucleophilic attack on the HE-TPP radical may be thermodynamically mandatory for re-reduction of the lowest potential proximal cluster [82]. In other words, the proximal cluster with the lowest redox potential is reduced twice continuously, and the median and distal clusters seem not to participate in the intramolecular electron transfer.

This re-reduction cluster hypothesis is well consistent with the results of our EPR experiment. EPR signals on addition CoA to the HE-TPP radical (Fig. 2-6 A, traces 3) and on addition of dithionite (Fig. 2-6 A, traces 4) are absent. In addition, the absorbance around 410 nm decreased on addition of CoA to the mixture of the wild type OFOR and pyruvate (Fig. 2-5 A, trace 5). Similar findings were made for the C197A mutant (Fig. 2-5 B, trace 5). These data suggest that the FeS cluster in StOFOR is re-reduced on addition of CoA, but the redox state after re-reduction remains unclear.

On the other hand, in the absence of external ferredoxin, the non-oxidative decarboxylation reaction proceeds (steps 9 and 10) at a much slower rate than the oxidative reaction, the HE-TPP being

protonated (step 9), and finally acetaldehyde is formed (step 10). The ability of non-oxidative decarboxylation was not basically affected by the intactness of the iron-sulfur cluster or the presence of CoA, which is different from in the case of the OFORs with three [4Fe-4S] clusters so far reported.

Figures and Tables

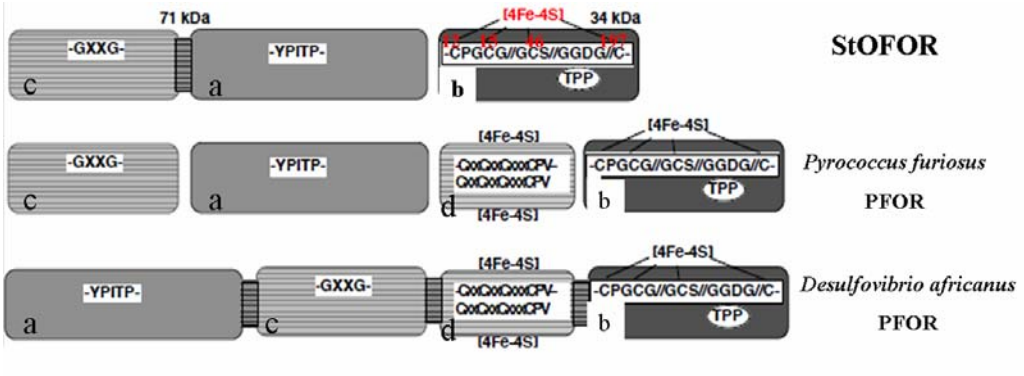

Fig.2-1. StOFOR is the simplest OFOR in the three types OFOR families.

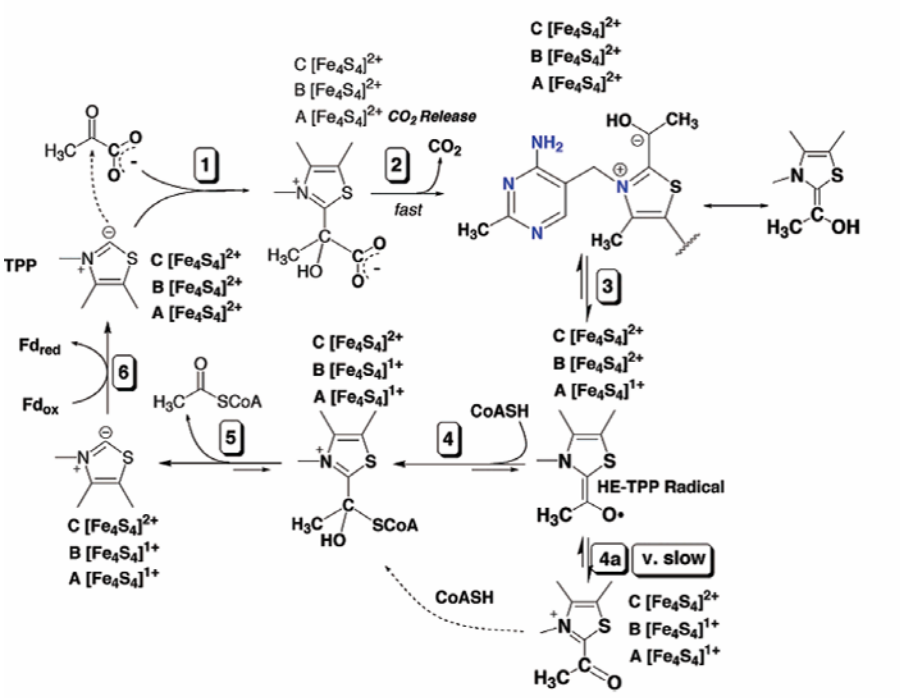

Fig.2-2. Reaction mechanism of homodimeric type PFORs [64].

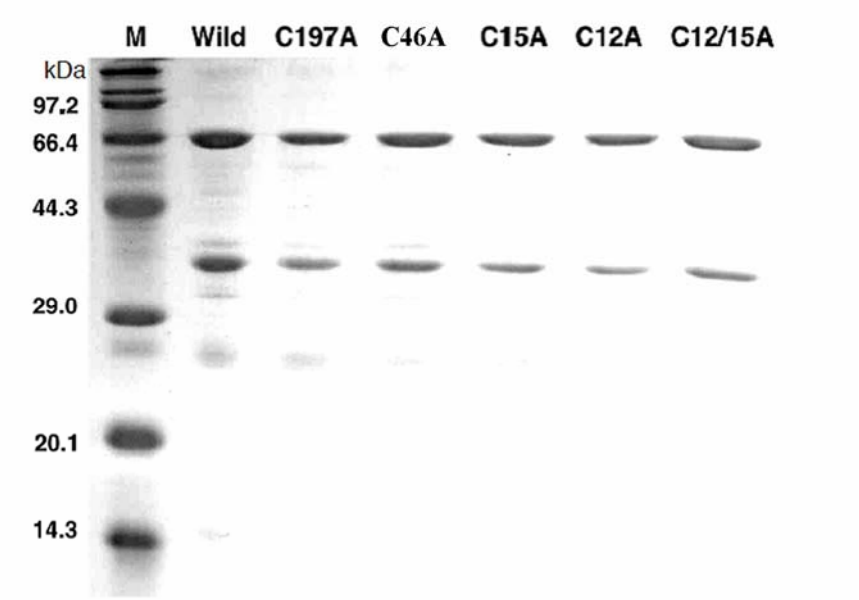

Fig.2-3. SDS-PAGE of the wild type and mutant StOFORs. M, molecular weight standards.

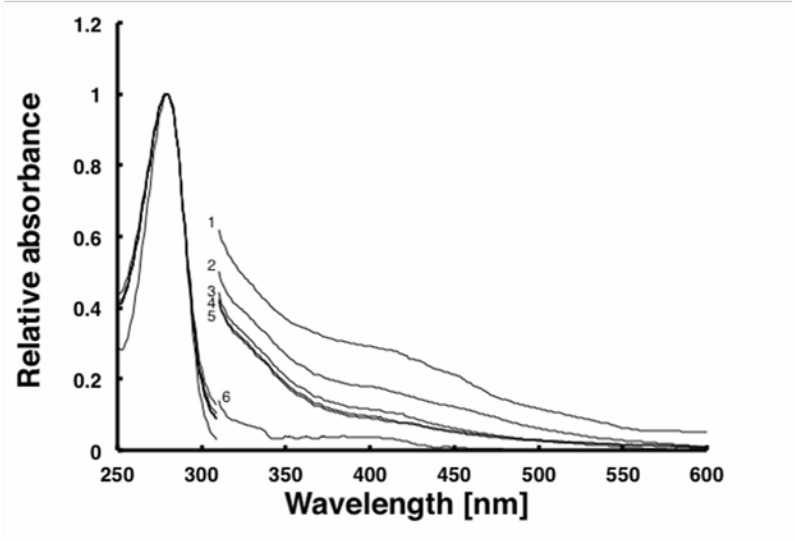

Fig.2-4. Absorption spectra of the wild type and mutant StOFORs. Relative absorbance was set at A_{280}=1 for each OFOR. Absorbance is enlarged 5-fold between 310 and 600 nm. Traces 1, 2, 3, 4, 5, and 6 are for the wild type, C197A, C46A, C15A, C12A, and C12/15A, whose concentrations were 0.72, 0.64, 0.58, 0.53, 0.55, and 0.51 mg/ml in 20 mM pH 7.5 Tris-Cl buffer, with maximal absorbance at 280 nm of 0.98, 0.87, 0.76, 0.65, 0.54 and 0.43, respectively.

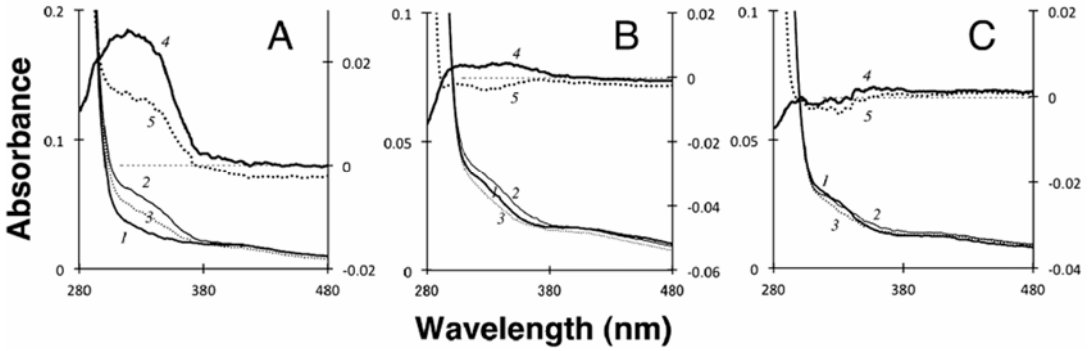

Fig.2-5. Absorption and difference spectra of wild type and mutant StOFOR2 between 280 and 480 nm. Traces 1, 2, 3, 4, and 5 are for the enzyme alone (0.7 mg/ml), enzyme + pyruvate (5mM), enzyme + pyruvate (5mM) + CoA (0.25mM), difference (2 - 1), and difference (3 – 1), respectively. (**A)** Wild type enzyme (0.7 mg/ml). (**B)** C197A (0.5 mg/ml). (**C)** C12A (0.45 mg/ml). The scales on the left and right are for absolute spectra (traces 1 – 3) and difference spectra (traces 4 and 5), respectively.

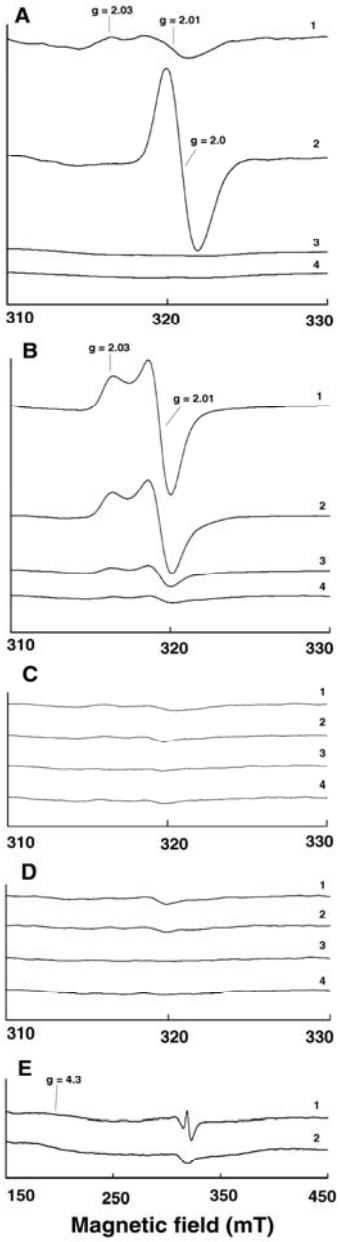

Fig.2-6. EPR spectra of wild type and mutant StOFORs. (A) wild type. (B) C197A. (C) C12A. (D) C12/15A. The instrument settings were: temperature, 8 K; microwave power, 1 mW; microwave frequency 8.991 GHz; modulation frequency, 100 kHz; and modulation amplitude, 0.8 mT Traces 1, 2, 3, and 4 are for the enzyme alone, enzyme + pyruvate (5mM), enzyme + pyruvate (5mM) + CoA (0.25mM), and enzyme + dithionite (5mM), respectively. (E) C197A (trace 1) and C12/15A (trace 2). The instrument settings were the same as above except for the temperature 14K.

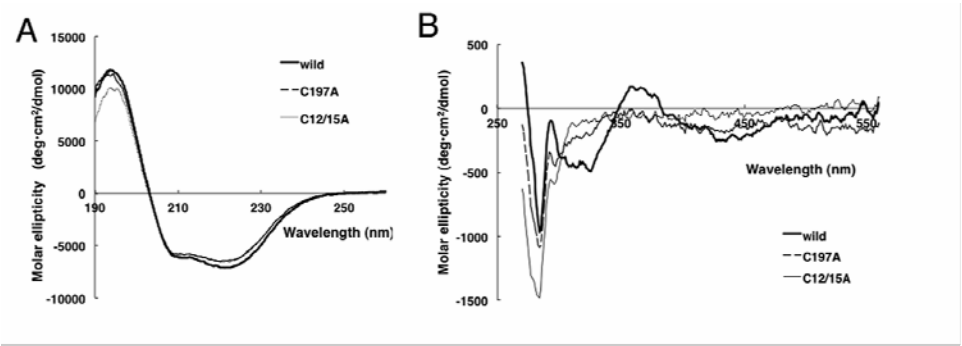

Fig.2-7. CD spectra of the wild type StOFOR, C197A and C12/15A in the far UV region. (A) and near UV-visible region (B) The protein concentrations and light paths are given under Materials and methods.

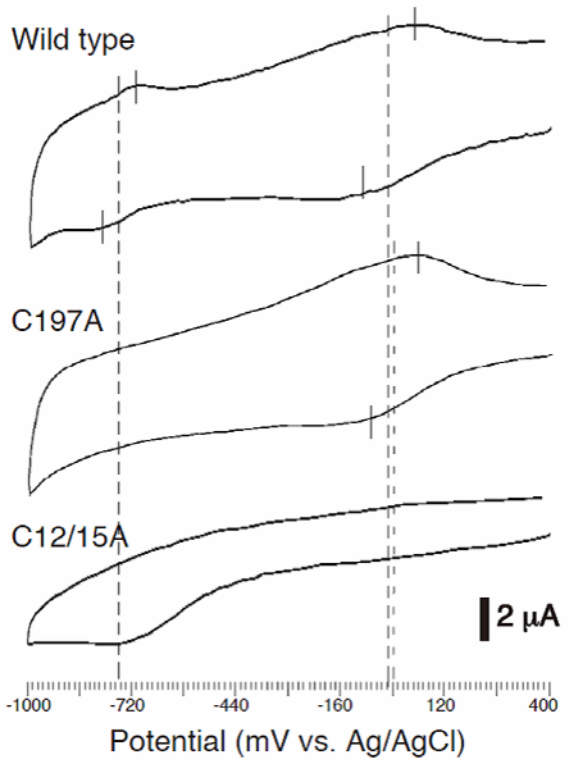

Fig.2-8. Cyclic voltammograms of the wild type StOFOR, C197A and C12/15A. Measured in 5 mM Tris-Cl, pH 7.5, containing 100 mM NaCl and 2 mM tobramycin as a promoter at 25˚C. See Materials and methods for details.

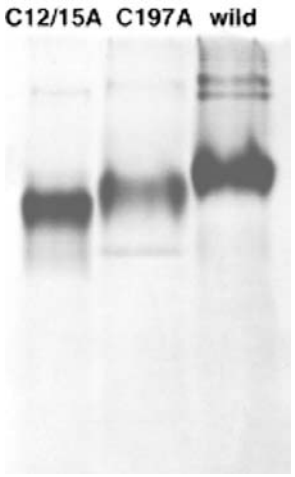

Fig.2-9. Native-PAGE of wide type and mutants StOFOR2

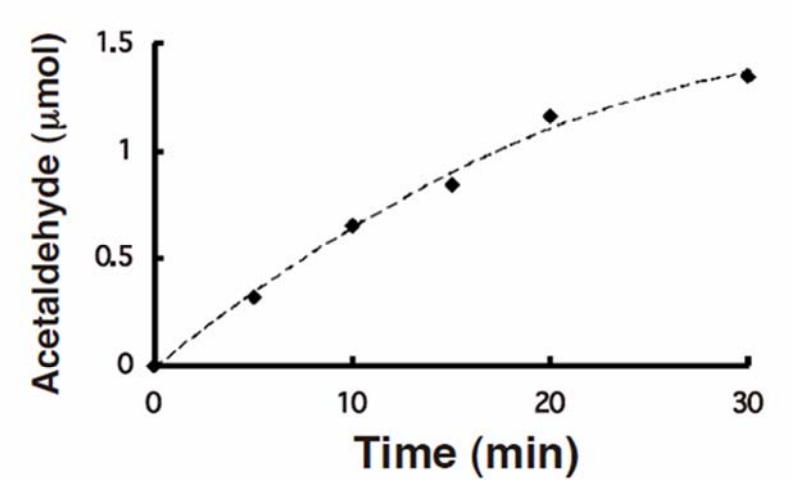

Fig.2-10. Time course of acetaldehyde production from pyruvate by StOFOR at 80˚C.

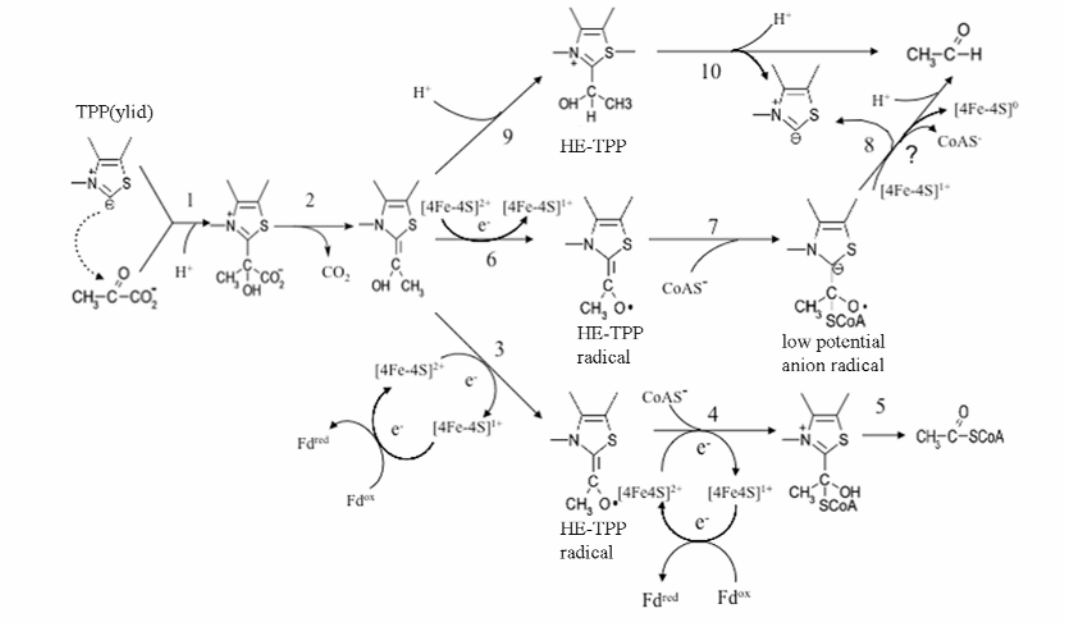

Fig.2-11. A revised reaction mechanism for StOFOR. See text for details.

Table.2-1. Oxidative decarboxylation of pyruvate with various electron acceptors.

	(A) Methylviologen[a]		(B) Cyt *c* reduction[b]			
	(U/mg)	(relative %)	+Fd (U/mg)	-Fd (U/mg)	net (U/mg)	net (relative %)
wild type	3.64	100	0.43	0.06	0.37	100
C197A	0.3	8	0.21	0.04	0.17	45.9
C46A	0.08	2.2	0.04	0.01	0.03	8.1
C15A	0.03	0.8	0.028	0.008	0.02	5.4
C12A	0.07	1.9	0.021	0.007	0.014	3.8
C12/15A	0.012	0.33	0.008	0.004	0.004	1.1

[a]Reduction of methylviologen measured anaerobically at 80℃. 1 U = 1 μmol/min.

[b]Reduction of bovine cytochrome *c* measured at 50℃. 1 U = 1 μmol/min.

See materials and methods for detailed conditions.

Table.2-2. Comparison of ability of non-oxidative decarboxylation between wild and mutant StOFORs.

	Acetaldehyde-producing activity (U/mg)[a]	
	with CoA (0.5 mM)	without CoA
Wild type	0.073	0.060
C197A	0.077	0.063
C46A	0.068	0.057
C15A	0.060	0.054
C12A	0.059	0.052
C12/15A	0.058	0.050

[a] 1 U=1 μmol/min at 80℃.

Chapter 3

Crystal structures of 2-oxoacid:ferredoxin oxidoreductases from *S. tokodaii*

本章の内容は、学術雑誌論文として出版する計画があるため公表できない。４年以内に出版予定。

Chapter 4

Ferredoxin:NADP$^+$ oxidoreductase from *S. tokodaii*

4-1 Introduction

Ferredoxin:NADP+ oxidoreductases (FNRs) are ubiquitous enzymes harbouring one molecule of noncovalently bound FAD as prosthetic group. They catalyze the reversible electron transfer between NADP(H) and the iron-sulfur protein ferredoxin (Fd) or FMN-containing flavodoxin [53, 54]. FNRs can be grouped into two phylogenetic/structural families that refer to as plant-type and glutathione reductase (GR)-type FNRs. Recently, a novel type of FNRs was reported, that is, thioredoxin reductase like FNRs (TRLFs), which physiologically function as FNRs, but exhibit a structural homology to NADPH-dependent thioredoxin reductases (TrxRs) [54-57]. The only reported enzyme that shows the FNR activity in archaea is called sulfide dehydrogenase from *P. furiosus*. However, it completely differs from the above three types of FNRs because of the subunit composition and prosthetic group [59].

StOFOR had been studied in catalyzing the CoA-dependent oxidative decarboxylation of 2-oxoacid to produce reduced ferredoxin (Fig. 4-1). In anaerobic archaea, recycling of reduced to oxidized ferredoxin is usually coupled to reduction of protons catalyzed by hydrogenases [89, 90], but this has not been clearly confirmed in aerobic archaea such as *S. tokodaii*, which lacks any hydrogenase. The only example is CYP119, a cytochrome P450 that catalyzes the monooxygenation of fatty acid in *Sulfolobales* using reduced Fd as an electron donor [91, 92].

We are interested in whether any of the above three (plant-, GR-, and TRLF-) types of FNRs function in the archaea. An ORF from *S. tokodaii*, ST2133, is annotated as a putative FNR. Its ortholog (Sso2222) in *S. solfataricus*, which shows 83% amino acid sequence identity with ST2133, has been characterized as a NADH oxidase [93]. Blast analysis of ST2133 revealed that the putative FNR exhibits high homology with thioredoxin reductases (TRs) although a Cys-x-x-Cys motif conserved in TRs is lacking [94-96] (Fig. 4-2).

In this chapter, I expressed ST2133 heterologously in *E. coli*, and characterized the purified product. The oligomeric state, and enzyme-bound-flavin species and content were analyzed. Comprehensive analyses of enzyme activities using the combination of NAD(P)H as an electron donor, and oxygen, hydrogen peroxide, 2,6-dichlorophenolindophenol (DCPIP), ferricyanide, cytochrome *c*, dithiobisnitrobenzoate (DTNB), or ferredoxin as an electron acceptor, were carried out. Electron transfer from reduced ferredoxin in *S. tokodaii* to $NADP^+$, and *vice versa*, was confirmed. Phylogenetic analysis revealed that ST2133 belongs to a novel type of TRLF with FNR activity. The possible role of ST2133 as a member of the redox cycle for ferredoxin is discussed.

4-2 Materials and methods

4-2-1 Plasmid and Bacterial strains

Recombinant plasmid pET28a-ST2133 with a His tag at its C-terminal was constructed using the primer set of 5'- GGAGATATACCATGGTAGTGATAGGA GGAGG-3' and 5'-GTGGTGGTGCTCGAGTTTTTTGAACTTATCCATTTC -3'. *E. coli* strain XL10 Gold was used for plasmid cloning. *E. coli* strain BL21 codon plus was used for plasmid expression.

4-2-2 Heterologous expression and purification of ST2133

Cells harboring the recombinant pET28a-ST2133 were grown in Luria-Bertani (LB)-Kanamycin (100 μg/ml) medium until OD600 reached 0.8 - 1.0 at 37℃. β-Isopropylthiogalactoside (0.1 mM) was added and the cells were grown for a further 6 h at 30℃. The cells were collected and suspended in 50 mM Tris-HCl buffer, pH 8.0, and then disrupted by sonication. The lysed cell suspension was heated at 70℃ for 20 min to denature *E. coli* proteins. After centrifugation of the mixture to remove denatured proteins, the supernatant was subjected to Ni^{2+} affinity chromatography on a HisTrap FF crude 5 ml column (GE Healthcare). The column was washed with 50 mM Tris-HCl buffer, pH 7.5, and then the proteins eluted with 50 mM Tris-HCl containing 500 mM imidazole buffer, pH 7.5, were collected. Then, the sample was subjected to Superdex-200 column chromatography (GE Healthcare) with equilibration with 20 mM Tris-HCl and 250mM NaCl, pH 7.5.

4-2-3 Cofactor determination

Fluorescence spectrophotometry and high performance liquid chromatography (HPLC) were performed for determination of enzyme-bound flavins. The sample protein and standard FAD, FMN, or riboflavin (Sigma-Aldrich) were treated with trichloroacetic acid (10%, w/v) for 10 min, and then centrifuged at 15,000 x g for 10 min. The supernatant was subjected to HPLC and fluorescence analyses. The HPLC analysis was performed with a Waters 600 controller equipped with a Waters 2996 photodiode array detector and a PEGASILODS C18 column (4.6×250 mm). The mobile phase was acetic acid/methanol (70:30), at the flow rate of 1 mL/min. The absorbance at 254 nm was recorded. Fluorescence was measured with a spectrofluorometer, FP-6500 (JASCO), at excitation and emission wavelengths of 450 and 535 nm, respectively. The trichloroacetic acid supernatant was mixed with 0.1 M potassium phosphate (pH 7.5) and then the fluorescence was measured. Then, 0.1 ml of 1 M HCl was added to the mixture until the pH became 2, and the fluorescence intensity was measured again at the same wavelengths.

4-2-4 UV-visible absorption spectra

UV-visible absorption spectra of ST2133 and ferredoxin were recorded with a JASCO V-560 spectroscopy. The spectral change was used to follow the reduction of ferredoxin and oxidation of NADPH at 70℃. Spectra of reduced ferredoxin were recorded after the addition of a trace amount of dithionite.

4-2-5 EPR measurement

EPR spectra were measured with a JES-FA100 spectrometer. The temperature was controlled with a JEOL ES-CT470 cryostat system.

4-2-6 Enzyme activity assay

All the enzyme activities were evaluated spectrophotometrically with a JASCO V-560 spectrophotometer equipped with a thermo-controller. Most of the kinetic data were obtained through three parallel experiments, unless otherwise stated.

NAD(P)H oxidase was assayed at 70℃ by determining the initial rate of NAD(P)H oxidation. The reaction mixture comprised 0.1 M potassium phosphate (pH 7.5), 2 μM-0.2 mM NAD(P)H (Oriental

Yeast Co. Ltd.), 0.2 mM FAD or FMN (Sigma-Aldrich), and a sample enzyme (17.4 μg), in a final volume of 0.4 mL. The reaction was started by adding the enzyme, and followed as the decrease in absorbance at 340 nm (ε = 6220 M-1 • cm-1). One unit of enzyme was defined as the amount of enzyme that catalyzed the oxidation of 1 μmol of NAD(P)H /min at 70℃. The formation of hydrogen peroxide was determined by the method previously described [69, 97-99] with slight modifications; after the reaction for NAD(P)H oxidase, 0.6 mM 4-aminoantipyrine, 1.5 mM N-ethyl-N-(2-hydroxy-3-sulfopropyl)-3-methylaniline and 6 units peroxidase were added to the mixture. The reaction product was quantitated by measuring the absorbance at 555 nm. One unit of activity corresponds to the production of 1 μmol hydrogen peroxide per min.

NAD(P)H peroxidase was assayed at 70℃ by anaerobic determination in the presence of 50 mM hydrogen peroxide as an electron acceptor, the decrease in absorbance at 340 nm of NAD(P)H being estimated, as shown above, or the decrease in hydrogen peroxide being estimated, as follows [97]. The reaction mixture for NAD(P)H decrease assay comprised 0.1 M potassium phosphate (pH 7.5), 2 μM-0.2 mM NAD(P)H (Oriental Yeast Co. Ltd.), 0.2 mM FAD or FMN (Sigma-Aldrich), 50 mM hydrogen peroxide, and a sample enzyme (17.4 μg), in a final volume of 0.4 mL. The reaction was started by adding the enzyme, and the reaction was followed by measuring the decrease in absorbance at 340 nm. One unit of activity was defined as the amount of enzyme that catalyzed the oxidation of 1 μmol of NAD(P)H/min at 70℃. The reaction mixture for the hydrogen peroxide consumption assay comprised 0.1 M potassium phosphate (pH 7.5), 0.2 mM NAD(P)H, 0.2 mM FAD or FMN, 50 mM H_2O_2 and a sample enzyme (17.4 μg), in a final volume of 0.4 mL. The reaction was started by adding the enzyme, and at the end of the linear decrease in absorbance at 340 nm at 70℃, the reaction mixture was cooled on ice to stop the reaction and subjected to hydrogen peroxide determination as described previously [69, 97-99].

Diaphorase activity was assayed at 70℃ by monitoring the reduction of DCPIP or ferricyanide as the decrease in absorbance at 600 nm (ε = 21.8 mM^{-1} •cm^{-1}) for DCPIP or 420 nm (ε = 1.0 mM^{-1} •cm^{-1}) for ferricyanide. The reaction mixture comprised 0.1 M potassium phosphate, pH 7.5, 0.1 mM DCPIP

or 1mM ferricyanide, and 2 μM-0.2 mM NAD(P)H, 0.2 mM FAD or 1 mM FMN, in a final volume of 0.4 mL. The reaction was started by adding the enzyme (8.7 μg), and the activity was calculated by subtracting the blank rate obtained in the absence of the enzyme. One unit of activity was defined as the amount of enzyme that catalyzed the oxidation of 1 μmol of DCPIP or ferricyanide per min at 70 ℃.

Cytochrome *c* reduction activity was assayed at 50℃ by montoring the increase in absorbance at 550 nm (ε = 27.8 $mM^{-1} \cdot cm^{-1}$) [57]. The reaction mixture comprised 0.1 M potassium phosphate, pH 7.5, 50 μM horse heart cytochrome c (Sigma-Aldrich), and 2 μM-0.2 mM NAD(P)H, 0.2 mM FAD or 1 mM FMN, and a sample enzyme (8.7 μg) in a final volume of 0.4 mL. One unit of activity was defined as the amount of enzyme that catalyzed the oxidation of 1 μmol of cytochrome *c* /min at 55℃.

Ferredoxin reduction activity was assayed by coupling with reduction of cytochrome *c* at 550 nm and 50℃ as described above. The blank value without ferredoxin was substracted to calculate the ferredoxin reduction activity. Ferredoxin (StFd, ST0163) was prepared from an *S. tokodaii* cell extract as previously reported [28].

DTNB reductase activity was evaluated as dithiobisnitrobenzoate (DTNB) reduction, and the formation of the product 2-nitro-5-thiobenzoate (TNB) was followed spectrophtometrically as the increase in absorbance at 412 nm (ε = 7.68 $mM^{-1} \cdot cm^{-1}$) [94]. The reaction mixture comprised 0.1 M potassium phosphate, pH 7.5, 5 mM DTNB, 2 μM-0.2 mM NAD(P)H, 0.1 mM FAD or FMN and 10 mM EDTA, and a sample enzyme (34.8 μg) in a final volume of 0.4 mL. One unit of activity was defined as the amount of enzyme that catalyzed the oxidation of 1 μmol of DTNB /min at 70℃.

Ferredoxin:$NADP^+$ oxidoreductase activity was determined by measuring the formation of NADPH from $NADP^+$ using reduced StFd as the electron donor under aerobic and anaerobic conditions. Reduced StFd was generated using StOFOR prepared as described previously [42, 50-52]. The standard reaction mixture comprised 0.1 M potassium phosphate (pH 7.5), 20 μM StFd, 10 mM pyruvate, 0.25 mM CoA, 25 g StOFOR, and 2 μM- 1 mM NADP+, in a final volume of 0.4 mL. The assay temperature was 80℃. The reaction was initiated by adding 34.8 μg ST2133 as the final

component. For the anaerobic assay, O_2 was purged by N_2 in a sealed cuvette. The production of NADPH was measured at 340 nm and the molar absorbance of 6.2 $mM^{-1} \cdot cm^{-1}$ was used to calculate the concentration of NADPH. One unit of enzyme activity is equal to 1 mole NADPH produced per min.

4-3 Results

4-3-1 Molecular properties of ST2133

The structural gene encoding ST2133 consists of 999 bp and encodes a protein of 332 residues with a predicted molecular mass of 36.6 kDa. ST2133 was expressed in *E. coli* using the vector pET28a with a his-tag at its C-terminus. The recombinant enzyme was purified by heat treatment, Ni^{2+} affinity chromatography and gel filtration. After the gel filtration, the enzyme gave two protein fractions, small (about 10 % protein, designated as Fr1) and large (about 90 % protein, designated as Fr2) ones, at elution positions corresponding to molecular masses of 160 kDa and 63 kDa, respectively (Fig. 4-3A). The two peaks showed similar NADPH:DCPIP oxidoreductase specific activity. On SDS-PAGE, the two peaks appeared as a single band corresponding to an apparent molecular mass of 36 kDa (Fig. 4-3B), suggesting that ST2133 was expressed as both a homodimer and higher oligomer (possibly 4 - 6mer). The absorption spectrum of Fr2 enzyme showed peaks at 346, 385 and 476 nm, while Fr1 enzyme showed peaks at 392 and 474 nm (Fig. 4-3C), which are typical of flavoproteins. In order to identify the bound flavin species, both the Fr1 and Fr2 proteins were treated with trichloroacetic acid and the flavin released into the supernatant was determined. The pH-dependent fluorescence intensity ratios of Fr2 protein, Fr1 protein, standard FAD, FMN, and riboflavin at pH 7.5 versus pH 3.5 were 0.69, 0.76, 0.62, 1.33 and 1.36, respectively. The results of the C18-RP-HPLC analyses showed a single peak at the retention time of 2.61 min for both Fr2 and Fr1 proteins, while standard FAD, FMN and riboflavin showed peaks at 2.73, 7.99 and 15.2 min, respectively. These results indicate that both Fr2 (homodimer) and Fr1 (higher oligomer) possess the same cofactor, FAD, their stoichiometries being estimated to be 0.92 and 0.88 mol per subunit. Moreover, the higher

oligomeric and dimeric forms appear in dynamic equilibrium, because repeated gel filtration of Fr1 gave a similar elution profile to that in Fig. 4-3A (data not shown). The specific activities, such as NADPH oxidase, diaphorase, NADPH:ferredoxin oxidoreductase and ferredoxin:$NADP^+$ oxidoreductase were alomost the same between higher oligomeric and dimeric forms (data not shown). The slight difference in absorption spectra between higher oligomer and dimer (Fig. 4-3C) may occur from the interaction of bound FADs at the oligomer interface. Thus, Fr2 (homodimeric) enzyme was mainly used in the following experiments.

4-3-2 Enzymatic activities of ST2133.

The results of the comprehensive analyses for the redox activities of ST2133 are summarized in Table 4-1. All kinetic data were obtained through three parallel experiments.

NAD(P)H oxidase activity

ST2133 has the ability to oxidize NAD(P)H under aerobic conditions without any dye. Unlike Sso2222 showing no activity, ST2133 showed low activity (0.04 U/mg) toward NADPH even without the addition of FAD or FMN. The activity was enhanced to 0.55 and 5.52 U/mg on the addition of 0.2 mM FAD and FMN, respectively. It was unexpected that the stimulative effect exerted by FMN was several times higher than that by FAD, although 1 mol FAD bound to 1 mol enzyme. The K_m values for NADPH were 11.2, 13.8 and 14.3 μM, in the presence of 0 mM and 0.2 mM FAD, and 0.2 mM FMN, respectively. NADH was a poor electron donor, and its oxidation was hardly detected in the absence of FAD or FMN. ST2133 showed exceedingly lower NADH oxidation activity than that of NADPH oxidation, even when FAD or FMN was added (Table 4-1).

NAD(P)H peroxidase activity

ST2133 showed 0.24 U/mg of NADPH peroxidase activity in the presence of 0.2 mM FMN (Table 4-1). Similar level of NAD(P)H peroxidase activity has been reported in NADH oxidase/NADPH polysulfide oxidoreduxtase from *Thermococcus kodakaraensis* [97].

Diaphorase activity

It has been reported that Sso2222 was not able to catalyze the electron transfer from NAD(P)H to DCPIP or ferricyanide [93]. However, ST2133 catalyzed this reaction with high rates of 1.37 and 0.44 U/mg for DCPIP and ferricyanide, respectively. The addition of flavin had a similar activation effect as that on NAD(P)H oxidase activity, and the DCPIP reduction activity reached 21.8 U/mg in the presence of 1 mM FMN. The K_ms for NADPH were 8.1 and 9.87 μM in the presence of 0.1 mM DCPIP and 1 mM ferricyanide, respectively, which were almost the same as that (11.2 μM) for NAD(P)H oxidase activity. The K_m values increased slightly (about 20 – 30 %) on the addition of flavins, for both NAD(P)H oxidase and diahorase activities. NADH was a poor electron donor, and its oxidation was hardly detected in the absence of FAD or FMN (Table 4-1).

DTNB reductase activity

ST2133 exhibits a high amino acid identity with thioredoxin reductase despite its lack of the two active site Cys residues, and we demonstrated that the DTNB reductase activity (0.055 U/mg) was much lower than that of that genuine thiredoxin reductase (0.5 U/mg) which can be explained by the lack of two Cys residues at the active site of TR [94] (Fig. 4-2). Compared to those on other oxidation activities, the flavin coenzymes, FAD or FMN, had no stimulative effect on thioredoxin reductase activity, and the K_m value (55.8 μM) was several times higher than those for other oxidation activities. For the TRLF from *C. tepidum*, the activity of DTNB reductase specific for NADH is 4-5 times higher than that for NADPH [100], while for ST2133, the activity of DTNB reductase specific for NADPH is 3-4 times higher than that for NADH.

Reduction of cytochrome *c*

TRLFs have been reported to show NADPH:cyt *c* oxidoreductase activity, which is critical in the electron transfer chain of photosynthetic bacteria [57, 100]. Similar to other TRLFs, ST2133 also catalyzed NADPH-dependent cyt *c* reduction. Like other cytochrome *c* reductases, ST2133 preferred

NADPH, with a V_{max} value of 0.2 U/mg and a K_m value of 3.94 μM, to NADH. The addition of FAD and FMN increased the V_{max} to 0.66 and 7.37 U/mg, and the K_m to 5.23 and 7.1 μM, respectively.

Reduction of ferredoxin

Ferredoxin reduction activity was assayed using cytochrome *c* as the final electron acceptor as described under Materials and methods. The TRLF from *B. subtilis* was reported to show high ferredoxin reduction activity with NADPH (22.6 U/mg) [57, 100]. ST2133 showed activities of 3.72, 0.24, and 0.08 U/mg in the presence of 1 mM FMN, 0.2 mM and 0 mM FAD, respectively (Table 4-1).

Ferredoxin reduction was directly observed by monitoring the spectral change around 410 nm, which reflects the redox state of the iron-sulfur clusters. We found that ST2133 was able to reduce StFd with NADPH as the reductant (Fig. 4-4). A similar finding was reported for FNR from *Hydrogenobacter thermophilus* TK-6 [101]. Reduction of StFd in the presence of ST2133 and NADPH was also observed on X-band EPR spectroscopy (Fig. 4-5). The sharp EPR signal of StFd at g = 2.03, characteristic of a [3Fe-4S] cluster and a [4Fe-4S] cluster as previously reported [28], slightly decreased on the addition of ST2133. Upon further addition of 1 mM NADPH, the sharp peak at g = 2.03 was reduced by about 70%, demonstrating that ST2133 elicited NADPH:ferredoxin oxidoreductase activity. In this experiment, exogenous FMN was not added since it would interfere with the 3Fe center resonance, as it was pointed out in the previous report that EPR elicited NADH dependent ferredoxin reduction of NADH oxidase from *Acidianus ambivalens,* a thermoacidophilic archaea belonging to the genus *Sulfolobales* [102].

Ferredoxin:$NADP^+$ oxidoreductase (FNR) activity

The FNR activity was assayed using an OFOR-coupled supply of reduced ferredoxin under aerobic and anerobic conditions. Each component of the standard reaction mixture (pyruvate, CoA, StOFOR, StFd, $NADP^+$ and ST2133) was necessary for activity (Figs. 4-6 A and C). Under aerobic condition, NADPH production was hardly linear and began to decrease after about 3 min (Fig. 4-6 B,

trace b, c, d), while under anaerobic condition, time course of NADPH production was linear and reached plateau when $NADP^+$ was consumed (Fig. 4-6 D), possibly because of the removal of interference of NADPH oxidase activity. The initial velocity was about ten times faster in anerobic than aerobic conditions. From the insets of Figs. 4-6 B and D, the K_m value for $NADP^+$ of 0.010±0.002 mM and the V_{max} of 0.13±0.01 U/mg for aerobic assay, and the K_m value for $NADP^+$ of 0.017±0.002 mM and the V_{max} of 1.33±0.06 U/mg for anerobic assay were determined.

4-4 Discussion

4-4-1 Oligomeric state

The recombinant enzyme, which is encoded by ST2133, exhibited a similar UV-visible spectrum of flavoenzymes to those of other FNRs and possesses one mole FAD per subunit as a cofactor [100, 103-105]. Similar with other TRLFs, ST2133 appears as a homodimer (63 kDa) in the main state and small amount of higher oligomer were also observed. Although the apparent MW of 63k is less than the theoretical value (73.2 k), such a behavior of oligomeric enzymes from hyperthermophiles is often observed because of the compact package of the quarternary structure [106-108].

Genes *st2133* and *st2132* (both in complementary strand) show 4-base overlap. Orthologous genes *sso2222* and *sso2223* from *S. solfataricus* show 68-base overlap. Transcriptome analysis of *sso2222* and *sso2223* has been reported [109]. According to the paper, transcription level ratio of neither *sso2222* nor *sso2223* is affected by the carbon source of growth media (YT or glucose). Transcription factor binding sites (palindromic) are found just before both *sso2222* and *sso2223*, and promoter sequences are more abundantly found in the upstream region of *sso2222* than that of *sso2223* (USCS Genome Browser on *S. solfataricus*, http://microbes.uscs.edu). Based on the above information, it is likely that *sso2222* and *sso2223* are co-transcribed. Nevertheless, proteome analysis showed that only Sso2222 but not Sso2223 is found in the cytosol [109]. Likewise, in the case of *S. tokodaii*, only ST2133 but not ST2132 is identified (http://www.bio.nite.go.jp/dogan/project/view/ST). Thus we consider that *st2133* and *st2132* are possibly co-transcribed but only *st2133* (or *sso2222*) is translated,

or if *st2133* or *sso2222* were translated, the product would be so small in amount or so unstable as to be detected.

Since *st2133* and *st2132*, which may encode a counterpart of ST2133 just as the case of *P. furiosus* heterodimeric FNR, are overlapped, the co-expression system of these genes was constructed on the basis of co-expression strategy for heterodimeric StOFOR [50], but production of heterodimer was not observed. Single expression of *st2132* gene resulted in accumulation of the gene product insoluble fraction (data not shown). Thus, the role of ST2132 was not clear, but it is important that ST2133 alone showed clear enzymatic functions. Overlap of the archaeal genes is often observed but it does not always imply that the products form heterodimer.

4-4-2 Catalytic properties

ST2133 showed oxidation activity specific for NADPH with various electron acceptors, such as molecular oxygen, DCPIP, ferricyanide, and cytochrome *c*. Even if a flavin was not added, low activity was observed for ST2133. This is inconsistent with the case of Sso2222, which is an ortholog of ST2133 with 83% amino acid identity. The native NADH oxidase encoded by Sso2222 did not show any activity without additional FAD, and this enzyme was not able to catalyze the electron transfer from NADH to DCPIP or ferricyanide [93]. The inconsistence between our data and those reported for the ortholog Sso2222 form *S. solfataricus* [93] could be due to the different pH of the assay and the his tag in the C-terminal of expressed protein, besides on the difference in the primary structure.

4-4-3 Intrinsic flavin and activation by exogenous flavins

Interestingly, although the flavin species of ST2133 is FAD, exogenous FMN exerts a several times higher activation effect than FAD. This feature is shared by the FNR from *Bacillus subtilis*, which belongs to the TRLF branch of the phylogenetic tree. When 0.1 mM FMN was exogenously added, the k_{cat} value of the NADPH oxidase activity was about two times higher than on incubation with 0.1 mM FAD, which is the natural cofactor of this enzyme [57]. No exchange of FAD with FMN was observed after incubation of ST2133 (10 mg/ml in 50 mM Tris-Cl, pH 7.5) and 2 mM FMN for

120 min at room temperature (data not shown). Since enzyme-bound FAD was not replaced by FMN, the mechanism of activation by FMN may be explained as the role of electron mediator of FMN from FAD to external receptor, as reported in the case of ferric reductase activity of FNR from *Pseudomonas putida* [110].

4-4-4 Coenzyme specificity

Chlorobium tepidum FNR uses both NADH and NADPH without significantly discriminating between them, and *Bacillus subtilis* FNR is far more specific for NADPH than NADH [57, 100]. ST2133 showed high specificity for NADPH, and the activity with NADH was hardly observed without the addition of an external flavin, whereas Sso2222 oxidized NADH and, less efficiently, NADPH, with the formation of hydrogen peroxide [93]. This indicates that ST2133 and Sso2222 are likely to play different roles in the regeneration of $NAD(P)^+$ from NAD(P)H produced during aerobic cellular metabolism. It has also been reported that FNRs specific for NADPH may play a role in responses to oxidative stress, although the molecular mechanism is still not clear. *E. coli* FNRs participate in cellular defence against oxidative damage, and FNR-deficient mutants are abnormally sensitive to hydrogen peroxide [111, 112]. A similar enzymatic system against oxidative stress has been reported for *H. thermophilus*. This system, composed of a NADPH-dependent FNR and a novel rubrerythrin-like protein called ferriperoxin, shows specific peroxidase activity toward both hydrogen peroxide and organic hydroperoxides [113].

The most striking finding in this study is that ST2133 is a reversible FNR with specific activities of 0.13 and 1.33 U/mg in forward aerobic and anerobic direction, respectively (without FMN, Fig. 4-6 B), and 3.72 U/mg in reverse direction (with FMN, Table 4-1). This is the first reported FNR activity for a crenarchaea. To our knowledge, the only reported FNR activity for an archaea is accompanied by sulfide dehydrogenase from *P. furiosus* [58, 59]. However, it exhibits little homology with the classical FNRs, such as the plant-, GR- and TRLF-types (Fig. 4-7).

4-4-5 Phylogenetic tree

Blast analysis of ST2133 revealed significant levels of identity with TR and FNR. Amino acid sequence alignment of ST2133 associated with related enzymes is shown in Fig. 4-2. The orthologous protein from *S. solfataricus* called *Sso*2222, which exhibits 83% amino acid identity with ST2133, has been characterized as NADH oxidase [93], but Sso2222 or ST2133 showed little homology with other NAD(P)H oxidase sequences available in the GeneBank data base. The best alignment was observed with TR and FNR. ST2133 exhibits about 40 - 50% identity with TRLFs such as the FNRs from *Chlorobaculum tepidum* and *Bacillus subtilis*, and all the TRLFs share conserved motifs that participate in FAD and NAD(P)H binding with TR from *E. coli* or *S. solfataricus*. However, TRLFs do not contain a Cys-x-x-Cys motif conserved in the active site of TRs (Fig. 4-2).

A phylogenetic tree of ST2133, plant-type FNRs, GR type FNRs, TRLFs and thioredoxin reductases is shown in Fig. 4-7, in which ST2133 and Sso2222 are more closely related to TRLFs than FNRs of the plant and GR types. Thioredoxin reductases including bacterial TRs and archaeal TRs are located between TRLFs and classical FNRs in the phylogenetic tree. ST2133 and Sso2222 branch earlier than other reported TRLFs, and are closer to the thioredoxin reductase branch. The structure (2ZBW) of a thioredoxin reductase like protein (TRLP) from *Thermus thermophilus*, which exhibits 50% amino acid identity with ST2133, has been reported, and recently designated as FNR [114]. We thus conclude that ST2133 can be classified as the novel type of thioredoxin reductases like FNRs.

In this study, we demonstrated that ST2133, annotated as a possible FNR, belonging to thioredoxin reductase-like enzyme (TRLE), does function as a ferredoxin:$NADP^+$ oxidoreductase, and plays an important role in the redox cycle of ferredoxin in the archaea; in the central metabolism of heterotrophically grown *S. tokodaii*, StOFOR catalyzes the conversion of both pyruvate, a glycolysis product, into acetyl-CoA, and 2-oxoglutarate, a member of the TCA cycle, into succinyl-CoA [42, 50-52], with simultaneous reduction of ferredoxin. The reducing power of ferredoxin is coupled with NADPH formation by ST2133 FNR (Fig. 4-6).

Fig. 4-8 summarizes the physiological role of FNR in *S. tokodaii* metabolism. NADPH is utilized

for various anabolic reactions such as lipid biosynthesis catalyzed by β-ketoacyl-ACP reductase (ST0070, ST1109, and ST1868) and HMG-CoA reductase (ST1352), and amino acid biosynthesis catalyzed by pyrroline-5-carboxylic reductase (ST0646), aspartate-semialdehyde dehydrogenase (ST1242), and homoserine dehydrogenase (ST1519). NADPH is also required in autotrophic metabolism such as in CO_2 fixation through reverse formation of reduced ferredoxin, which in turn fixes CO_2 and acyl-CoA into 2-oxoacid, or by malonyl-CoA reductase/succinyl-CoA reductase (ST2171), malonate semialdehyde reductase (ST1507), succinate-semialdehyde reductase (ST2056), acryloyl-CoA reductase (ST0480), and gluconeogenesis catalyzed by glyceraldehyde 3-phosphate dehydrogenase (ST1356) [115], as suggested from the reference [12].

Figures and Tables

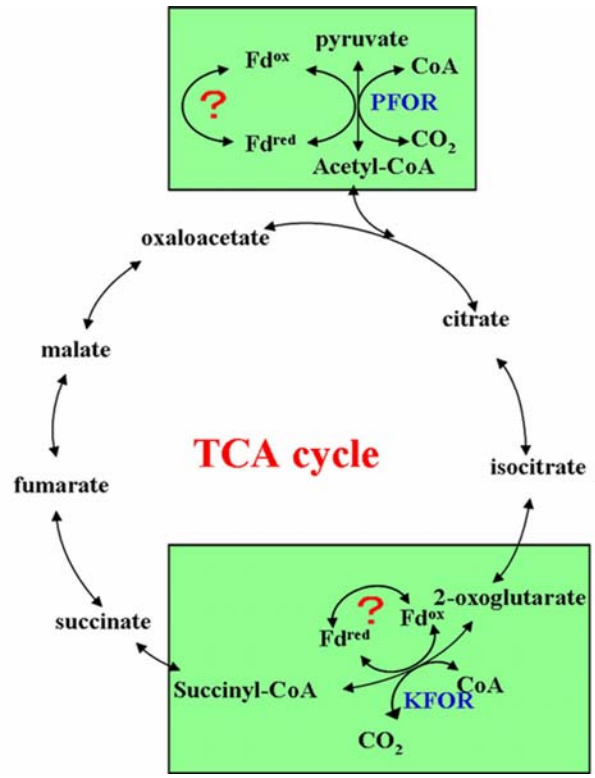

Fig.4-1. The TCA cycle in *S.tokodaii*.

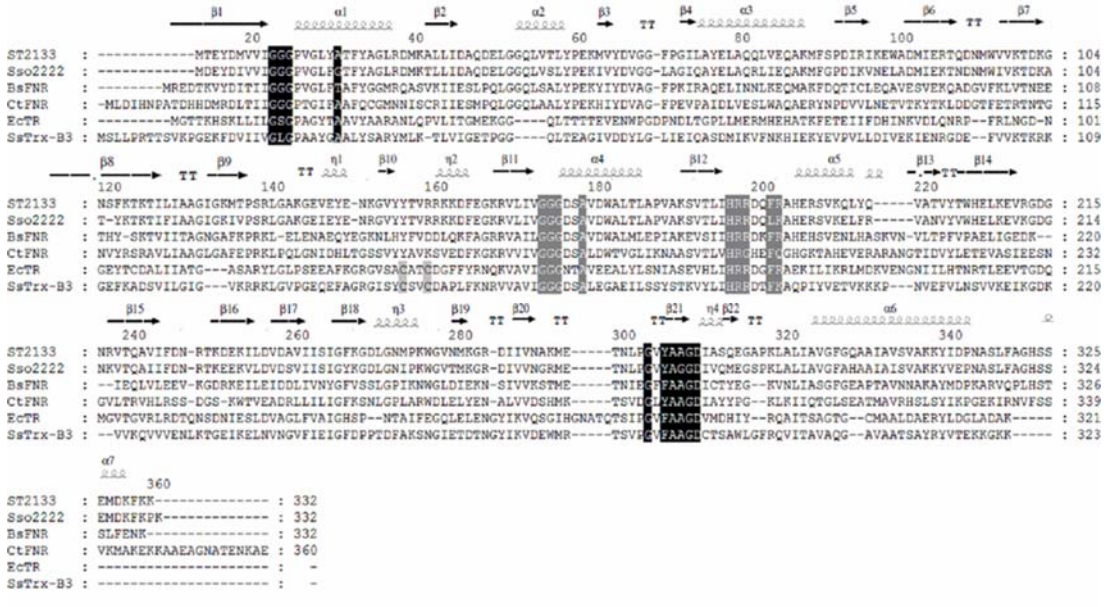

Fig.4-2. Multiple alignment of the amino acid sequence of ST2133 with those of Sso2222 from *S. solfataricus*, FNR from *Chlorobaculum tepidum* (CtFNR), FNR from *B. subtilis* (BsFNR), TR from *E. coli* (EcTR) and TR from *S. solfataricus* (SsTrx-B3). Residues involved in the FAD binding are highlighted in black boxes. The Cys consensus sequence is gray shadowed. Residues involved in NADP binding are highlighted in gray boxes.

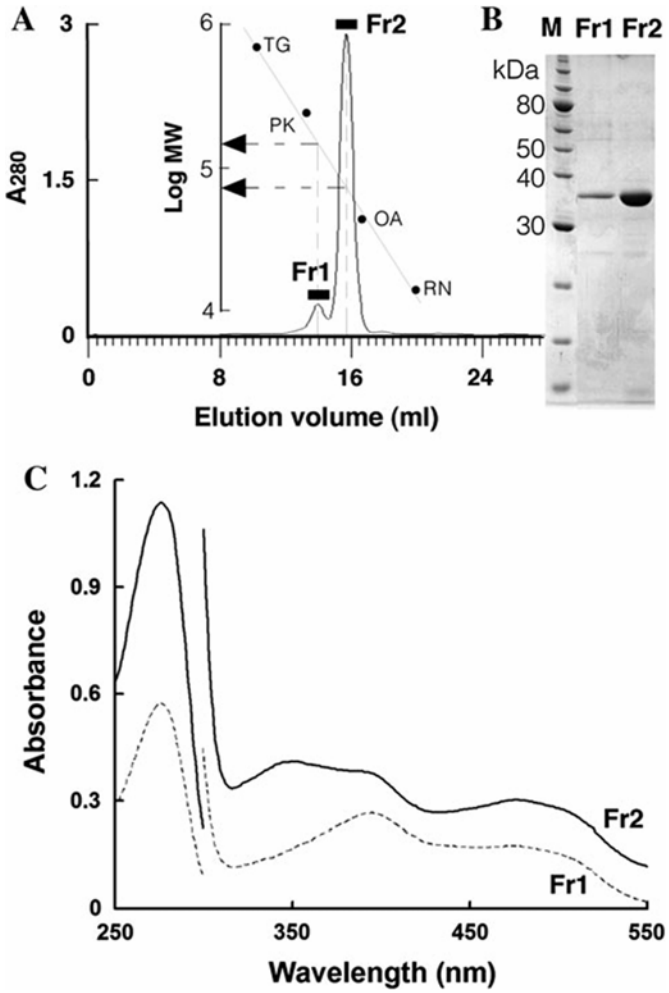

Fig.4-3. Two forms of ST2133. (A) Elution profile of gel filtration chromatography and calibration of MW using standard proteins: TG, thyroglobulin, 669 k; PK, pyruvate kinase, 237k; OA, ovalbumin, 44k; RN, RNaseA, 14k. (B) SDS-PAGE of Fr1, Fr2 and MW standards (M). (C) Absorbance spectra of Fr1 (0.4 mg protein / ml) and Fr2 (1.0 mg protein / ml) in 20 mM Tris-HCl (pH 7.5). The spectra between 300 nm and 550 nm are enlarged by 5-fold.

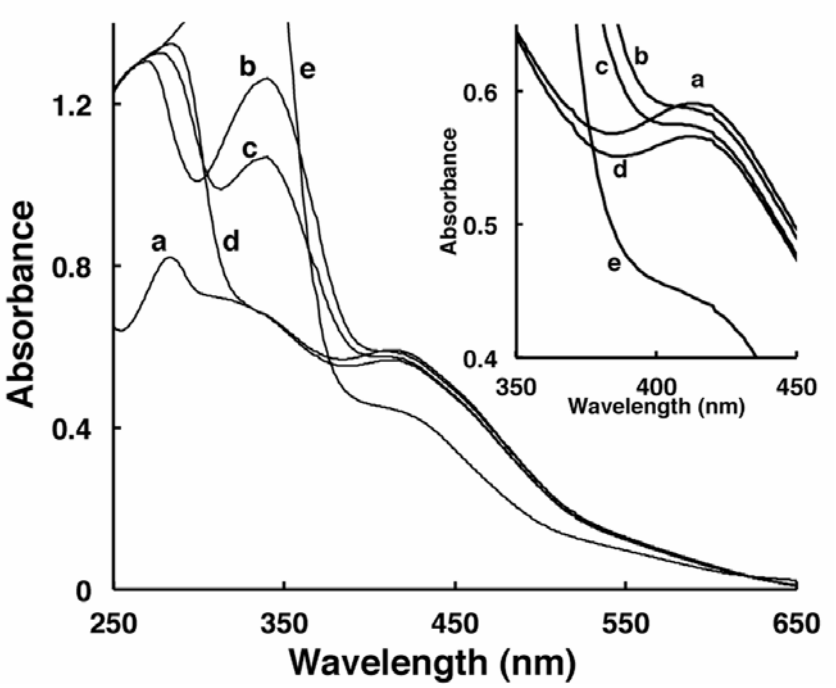

Fig.4-4. UV-visible spectral change of ferredoxin. The spectra were measured at 70℃ under aerobic conditions. The spectra are enlarged between 350 nm and 470 nm (inset). Trace *a*, 20 μM ferredoxin from *S. tokodaii*. Trace *b*, *a* plus 0.2 mM NADPH. Trace *c*, *b* plus 0.02 mg ST2133. Trace *d*, *b* plus 20 g ST2133 after 15 min at 70℃. Trace *e*, *d* plus 0.2 mM dithionite.

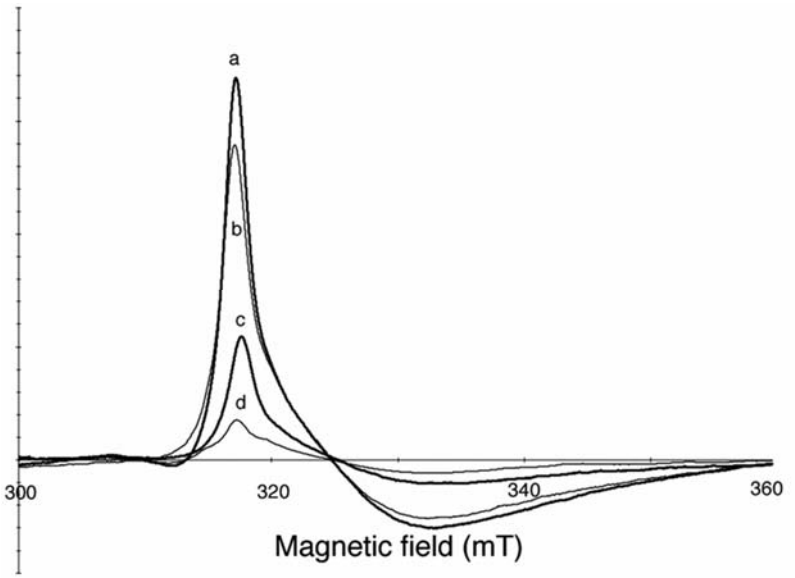

Fig.4-5. EPR spectra of ferredoxin from *S. tokodaii* and its reduction by ST2133 in the presence of NADPH. Trace *a*, 20 μM ferredoxin in 20 mM potassium phosphate buffer, pH 7.0. Trace *b*, 20 μM ferredoxin plus 15 μg ST2133 in 20 mM potassium phosphate buffer, pH 7.0, 15 min at 37˚C. Trace *c*, 20 μM ferredoxin, 15 μg ST2133 and 1 mM NADPH in 20 mM potassium phosphate buffer, pH 7.0, 15 min at 37˚C. Trace *d*, 20 μM ferredoxin plus sodium dithionite. EPR spectra were measured at 4K with a

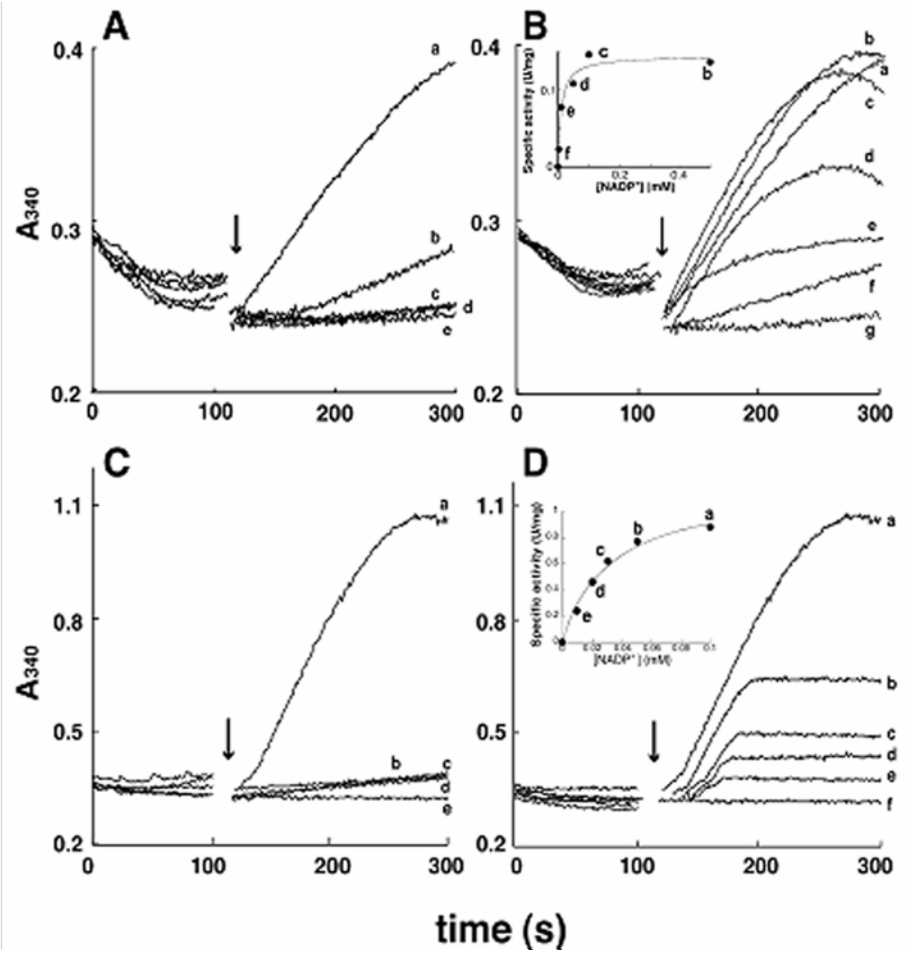

Fig.4-6. Ferredoxin:$NADP^+$ oxidoreductase activity of ST2133 measured aerobically (A, B) and anaerobically (C, D). (A) Trace *a*, the standard reaction mixture comprised 0.1 M potassium phosphate (pH 7.5), 20 μM StFd, 10 mM pyruvate, 0.25 mM CoA, 25 μg StOFOR, and 1 mM $NADP^+$. Trace *b*, the standard reaction mixture without CoA. Trace *c*, the standard reaction mixture without pyruvate. Trace *d*, the standard reaction mixture without OFOR. Trace *e*, the standard reaction mixture without ferredoxin. (B) Relationship between the concentration of $NADP^+$ and the FNR activity. Traces *a*, 1 mM; *b*, 0.5 mM; *c*, 0.1 mM; *d*, 0.05 mM; *e*, 0.01 mM; *f,* 0.0025 mM; *g*, 0 mM $NADP^+$. (C) Trace *a*, the standard reaction mixture comprised 0.1 M potassium phosphate (pH 7.5), 20 μM StFd, 10 mM pyruvate, 0.25 mM CoA, 25 μg StOFOR, and 1 mM $NADP^+$. Traces *b*-*e*, the same as in (A). (D) Relationship between the concentration of $NADP^+$ and the FNR activity. Traces *a*, 0.1 mM; *b*, 0.05 mM; *c*, 0.03 mM; *d*, 0.02 mM; *e*, 0.01 mM; *f,* 0 mM $NADP^+$. Arrow indicates the addition of ST2133 (34.8 μg in aerobic and 31.2 μg in anaerobic condition).

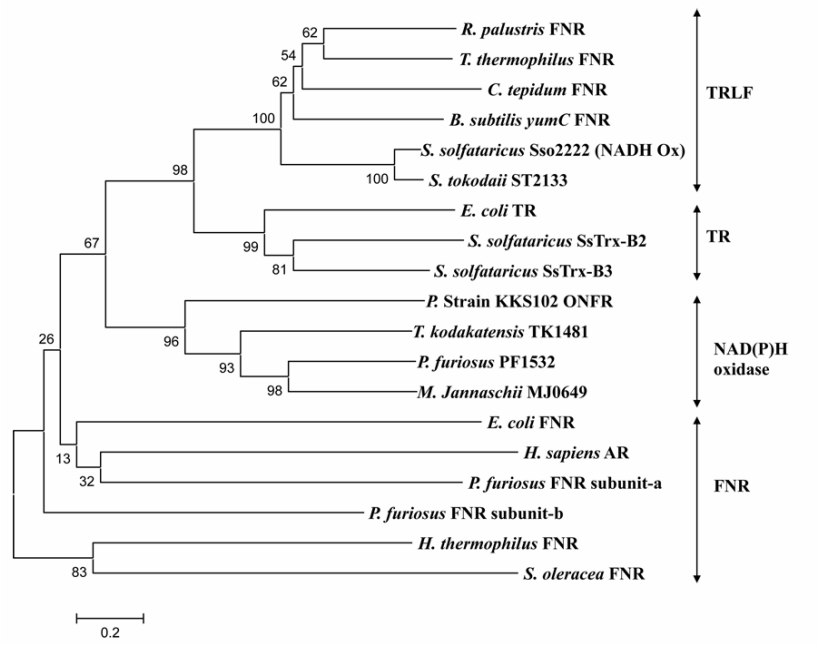

Fig.4-7. Phylogenetic tree of ST2133 and related enzymes. The sequences were aligned using CLUSTALX 2 and a tree was constructed using the neighbor-joining method on MEGA 5. Bootstrap values after 1000 resamplings are indicating as percentages on the corresponding branches. The lower scale indicates the relative distance between nodes. *R. palustris, Rhodopseudomonas palustris*; *T. thermophilus*, *Thermus thermophilus*; *C. tepidum*, *Chlorobaculum tepidum*; *B. subtilis, Bacillus subtilis*; *S. solfataricus*, *Sulfolobus solfataricus*; *S. tokodaii, Sulfolobus tokodaii*; *E. coli, Esherichia coli*; *P.* strain KKS102, *Pseudomonas* SP. strain KKS102; *T. kodakatensis*, *Thermococcus kodakatensis*; *P. furiosus*, *Pyrococcus furiosus*; *M. jannaschii*, *Methanocaldococcus jannaschii*; *H. sapiens*, *Homo sapiens*; *H. thermophilus*, *Hydrogenobacter thermophilus*; *S. oleracea*, *Spinacia oleracea*. AR, adrenodoxin reductase; ONFR, oxygenase-coupled NADH-ferredoxin reductases.

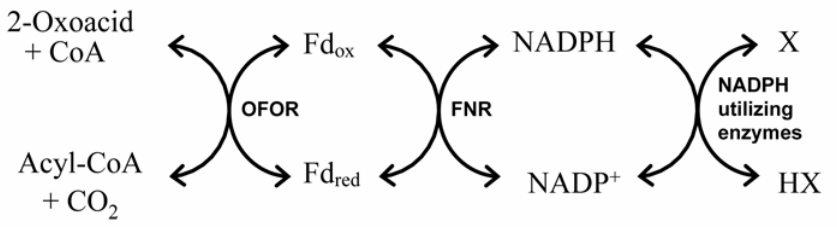

Fig.4-8. Putative physiological status of ST2133. Possible $NADP^+$ utilizing enzymes are listed in the text.

Table 4-1. Summary of the enzyme activities of ST2133.

Electron donor	Addition	V_{max}[a] and K_m[b]	NADPH oxidase (70℃, aerobic)		NADPH peroxidase (70℃, anaerobic)		Diaphorase activity (70℃)		Cyt *c* reduction (55℃)	Fd[c] reduction (55℃)	DTNB reductase (70℃)
			NADPH oxidation (340 nm)[d]	H_2O_2 formation	NADPH oxidation (340 nm)[d]	H_2O_2 consumption	DCPIP reduction (600 nm)[d]	Ferricyanide Reduction (420 nm)[d]	cyt *c* reduction (550 nm)[d]	Fd dependent cyt *c* Reduction (550 nm)[d]	DTNB reduction (412 nm)[d]
NADPH (0.2 mM)	**None (E only)**	V_{max} / K_m	0.04±0.007 /11.23±0.52	0.03±0.008	0.02±0.005 /24.13±1.21	0.03±0.01	1.37±0.04 /8.1±0.87	0.44±0.02 /9.87±1.02	0.2±0.01 /3.94±1.04	0.08±0.01 /6.32±0.93	0.055±0.003 /55.8±0.98
NADPH (0.2 mM)	**FAD (0.2 mM)**	V_{max} / K_m	0.55±0.08 /13.75±1.21	0.4±0.09	0.05±0.01 /27.12±1.45	0.04±0.007	4.36±0.12 /10.02±1.03	1.28±0.09 /10.43±1.42	0.66±0.03 /5.23±1.44	0.24±0.07 /6.84±1.05	0.049±0.006 /51.4±1.24
NADPH (0.2 mM)	**FMN (0.2 or 1 mM)**	V_{max} / K_m	5.52±0.93 /14.32±1.83	3.79±0.67	0.24±0.05 /26.13±1.41	0.21±0.04	21.8±1.29[e] /10.98±2.12	6.67±0.82 /11.12±1.95	7.37±0.45[e] /7.1±2.08	3.72±0.19[e] /7.21±1.12	0.048±0.008 /53.2±1.01
NADH (0.2 mM)	**None (E only)**	V_{max}	ND[f]	-	-	-	ND	-	ND	ND	0.012
NADH (0.2 mM)	**FAD (0.2 mM)**	V_{max}	ND	-	-	-	0.02	-	ND	0.02	0.014
NADH (0.2 mM)	**FMN (0.2 mM)**	V_{max}	0.01	-	-	-	0.03	-	0.01	0.04	0.015

[a] V_{max} in U/mg. [b] K_m for NADPH in μM. K_m and V_{max} are calculated by the method of Michaelis-Menten non linear fitting. [c] Difference in cyt *c* reduction rate between in the presence and absence of 20 μM Fd. [d] Wavelength at which the reaction was continuously monitored. [e] 1 mM FMN. [f] Nd, not detected.

Chapter 5

Ferredoxins from *Sulfolobus tokodaii* and *Aeropyrum pernix*

5-1 Introduction

S. tokodaii is a typical aerobic and thermoacidophilic archaea that grows optimally at pH 2-3 and 75-80℃. The archaea acquires biological energy by aerobic respiration rather than simple fermentation, and contains at least two different electron transport systems: One is the membrane-bound aerobic respiratory chain coupled at the level of succinate, and the other is the cytoplasmic ferredoxin (Fd)-dependent system coupled at the oxidative level of pyruvate and ketoglutarate [116, 117]. A dicluster-type Fd from *S. tokodaii* (StFd1 hereafter) have been characterized and the crystal structure has also been determined, and showing that a unique zinc-ligating Fd possess one [3Fe-4S] cluster and one [4Fe-4S] cluster [27]. In the course of large-scale preparations of StFd1, another Fd-like fractions was found in the DEAE chromatography (Fig.5-1), designated as StFd2 hereafter. In addition, there are two very similar *fd* genes (91% identity) in the genome of *S. tokodaii,* those are *st0163* and *st1175* (Fig.5-2A). It has been known that *st0163* encodes StFd1, and although StFd2 was isolated, sequenced and characterized as an alternative form of StFd1 in previous report, there were several ambiguous residues which has not been sequenced well including the 9th residue [116], which is an important difference in N-terminal region between *st0163* and *st1175* (Fig.5-2A). Thus, whether *st1175* encodes the StFd2 or not is an interesting question. There is a similar case that two *fd* genes (*ape0104a* and *ape0320*) also existed in the genome of *A. pernix*, but their cluster types are different: single cluster type and diclusters type, respectively, according to the number of cysteine residues (Fig.5-2B).

In this chapter, the above four *fd* genes were cloned and characterized, and their physiological functions were also discussed. Furthermore, StFd1 and StFd2 were isolated from crude extracts from *S. tokodaii*. They were sequenced and characterized, finally draws a conclusion that StFd2 is indeed alternative form or clusters damageable state of StFd1, which were suggested previously [116].

5-2 Materials and methods

5-2-1 Plasmid and Bacterial strains

The expression plasmid of St0163 (pUFD) [29], which was made by Dr. Kojoh, was used as a template to construct expression plasmids of other *fd* genes. According to the in-fusion cloning kit protocol (TaKaRa), insert of *st0163* were replaced by *st1175*, *ape0104a*, and *ape0320*, respectively. Sequences were confirmed by MACROGEN.

5-2-2 Heterologous expression and purification of various recombinant Fds

Cells harboring the recombinant various Fd plasmids were grown in Luria-Bertani (LB)-Kanamycin (100 μg/ml) medium until OD_{600} reached 0.8 - 1.0 at 37℃. β-Isopropylthiogalactoside (0.1 mM) and 0.1 mM $FeSO_4$ was added and the cells were grown for a further 20 h at 30℃. The cells were collected and suspended in 50 mM Tris-HCl buffer, pH 8.0 (designated as buffer I), and then disrupted by sonication. The lysed cell suspension was heated at 70℃ for 15 min to denature *E. coli* proteins. After centrifugation of the mixture to remove denatured proteins, the supernatant was loaded on to a DEAE Sepharose column. The column was eluted with a linear gradient of NaCl (from 0 to 0.4 M) in buffer I. The brown band was collected and made to 1.6 M with ammonium sulfate by adding a 3.2 M solution adjusted to pH 7.5 with Trizma base. The sample was applied to a Butyl-Toyopearl column pre-equilibrated with 1.6 M with ammonium sulfate in buffer I and eluted with a linear gradient of 1.6-0 M ammonium sulfate in buffer I. The brown band eluted was collected and concentrated with Centricon-10 (Amicon). The sample was subjected to Superdex-200 column chromatography, with equilibration with 0.25 M NaCl in buffer I. The sample thus prepared was used as purified Fds.

DEAE cellulose chromatography fractions derived from crudes extract of *S. tokodaii* were obtained from Dr. Wakagi. The following purification steps are identical with recombinant Fds. The sample thus prepared was used as purified StFd1 and 2.

5-2-3 Optical spectral analyses and EPR measurements

The procedures are the same as chapters 2-2-4 and 2-2-6

5-2-4 Activity assays

Fd activities were assayed by the coupling of various 2-oxoacid ferredoxin oxidoreductases (OFORs). The detailed methods are the same as chapter 2-2-3.

5-2-5 Protein sequence from N-terminal

Protein sequence from N-terminal was performed according to the methods of phenyl-isothiocyanate (Edman degradation). Firstly, the interest proteins were applied by SDS-PAGE, then proteins on the polyacrylamide gels were electrophoretically blotted transcript into PVDF membrane. Afterwards, the PVDF membrane were stained by quick CBB (Wako) and cut into a single bands. Lastly, the single bands were applied to Procise HT (Applied Biosystems) protein sequencer.

5-3 Results

5-3-1 Characterizations of various recombinant Fds

St0163 and *st1175* from *S. tokodaii* as well as *ape0104a* and *ape0320* from *A. pernix* were heterologously expressed and purified in *E.coli* as described in materials and methods. The purified products St0163, St1175, Ape0104a and Ape0320 showed a single band in 15% SDS-PAGE, corresponding to the molecular mass of approximately 11 kDa, 11 kDa, 8 kDa, and 12 kDa, respectively (Fig. 5-3). Although all of the four Fds exhibit brown colors, the relative absorbance in 410 nm of UV-visible absorbance spectra are different from each other. St0163 and Ape0104a showed similar lines of height in 410 nm, whereas St1175 and Ape0320 was decreased by 14.7% and 33.3%, respectively, suggest that the iron-sulfur clusters in St1175 and Ape0320 might exist in different states or partially degradedly exposure to oxygen (Fig. 5-4). St0163 and St1175 were characterized by EPR, and both of the Fds gave rise to a sharp peak at g = 2.03, characteristic of $[3Fe\text{-}4S]^{1+}$ cluster, while St0163 elicited a distinct shoulder in g = 1.98, which was not observed in ST1175 (Fig. 5-5). Similar result was also reported previously [116].

The physiological activities of three recombinant Fds (St0163, Ape0104a and Ape0320) were measured through using four recombinant OFORs (StOFOR1, StOFOR2, SsoOFOR and ApeOFOR1), which were successfully expressed and purified in chapter 3. Interestingly, the three *Sulfolobus*

OFORs (StOFOR1, StOFOR2, SsoOFOR) showed activities with not only St0163 but also Ape0320, which possess two clusters based on the amino acid sequence, while the activity was nearly not detected by the single cluster Fd (Ape0104a). Somehow expectedly, ApeOFOR1 showed activities by all of the three recombinant Fds regardless of their types (Table 5-1).

5-3-2 Isolation and characterization of two Fds from cytosol of *S. tokodaii*

The DEAE chromatography of *S. tokodaii* crudes extracts showed two separate Fd-like fractions (Fig. 5-1). The former fractions have been characterized as StFd1, and the structure has also been determined. The latter fractions were purified as described in materials and methods. However, in the butyl-chromatography and gel filtration, the brown color of latter fractions became less and less, and finally only gave rise to a small peak of brown color in gel filtration as shown in Fig. 5-6 fraction 8. Although fraction 6 and 7 showed the same position bands with fraction 8 in SDS-PAGE, the brown color could nearly not be observed, indicating that the iron-sulfur cluster has been completely destructed during purification. For the purification of StFd1, it was isolated in large amount as previously reported shown in the Fig. 5-6 fraction 5. StFd1 and 2 (Fraction 5 and 8) were characterized by UV-visible absorbance spectra, and fraction 8 decreased by about 37% in 410 nm, compared to fraction 5 (Fig. 5-7 line 1 and 2). The absorbance of fraction 8 in 410 nm extremely approach the reduced state of fraction 5 incubated with 10 mM dithionite (Fig. 5-7 line 3).

StFd1 and 2 (Fraction 5 and 8) were sequenced from N-terminal as described in materials and methods. Because of the only differences in 9th and 18th residues from N-terminal between St0163 and St1175 (Fig.5-2A), fraction 5 and 8 were sequenced from residues 2 to 19 of N-terminal, and the two Fds showed the same amino acid sequence with St0163 (Fig.5-8). Therefore, only Fds encoded by *st0163* could be isolated from the cytosol of *S. tokodaii*, and StFd2 is identical with StFd1 in primary structure, seems to be in aggregrated or damageable state of StFd1.

5-4 Discussions

In this chapter, various recombinant and natural Fds from *S. tokodaii* and *A. pernix* were prepared and characterized. For the *S. tokodaii* Fds, StFd1 encoded by *st0163* and its recombinant one were isolated in the largest amount and contained intact iron-sulfur clusters and showed high OFOR activity as previously reported [87]. Although StFd2 was also isolated from cytosol of *S. tokodaii*, it existed in an extreme unstable state, whose iron-sulfurs clusters easy to be degraded upon exposure to oxygen, which was previously proposed [116]. *St1175* might be a pseodugene, which has lost the ability to be transcribed or is no longer expressed in *vivo* of *S. tokodaii*. Two *fds* genes (*ape0104a* and *ape0320*) of *A. pernix* was also heterologously expressed in *E. coli*, and both of the purified products are iron-sulfur cluster-containing Fds, which showed activities assayed by *A. pernix* OFOR (ApeOFOR1).However, which one is the original electron acceptor of ApeOFOR1 can not be determined by this activity measurement. On the other hands, *Sulfolobus* OFORs only showed activities by using dicluster type Fds (Ape0320 and St0163) for some unknown reasons. In order to clarify this question, the redox potential of every OFORs and Fds will be assayed and compared, respectively, in the future. It is interesting to notice that StFd1 and StOFOR1 are abundantly present in the cytosol, while their paralogs, StFd2 and StOFOR2 are not translated in the gived condition, although their genes are conserved in the organism.

Figures and Tables

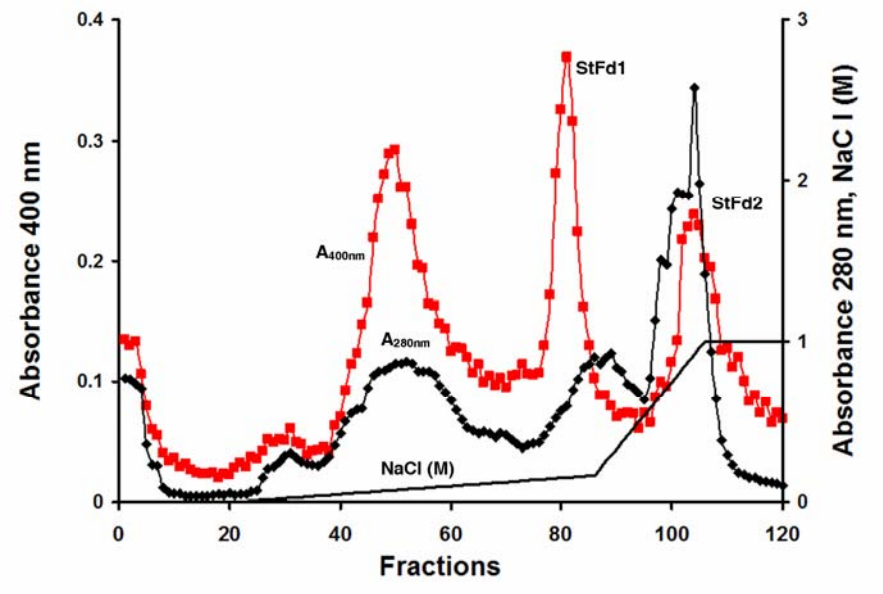

Fig.5-1. DEAE cellulose chromatography of extract crudes from *S. tokodaii*. Absorbance at 280 nm and 410 nm are shown by black and red lines, respectively.

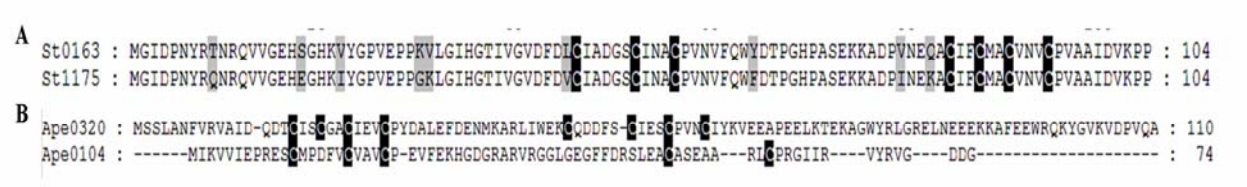

Fig.5-2. Amino acid sequence alignment of Fds. The Cys consensus sequence are highlighted in black boxes. (A) St0163 and St1175. The different residues are gray shadowed. (B) Ape0320 and Ape0104a

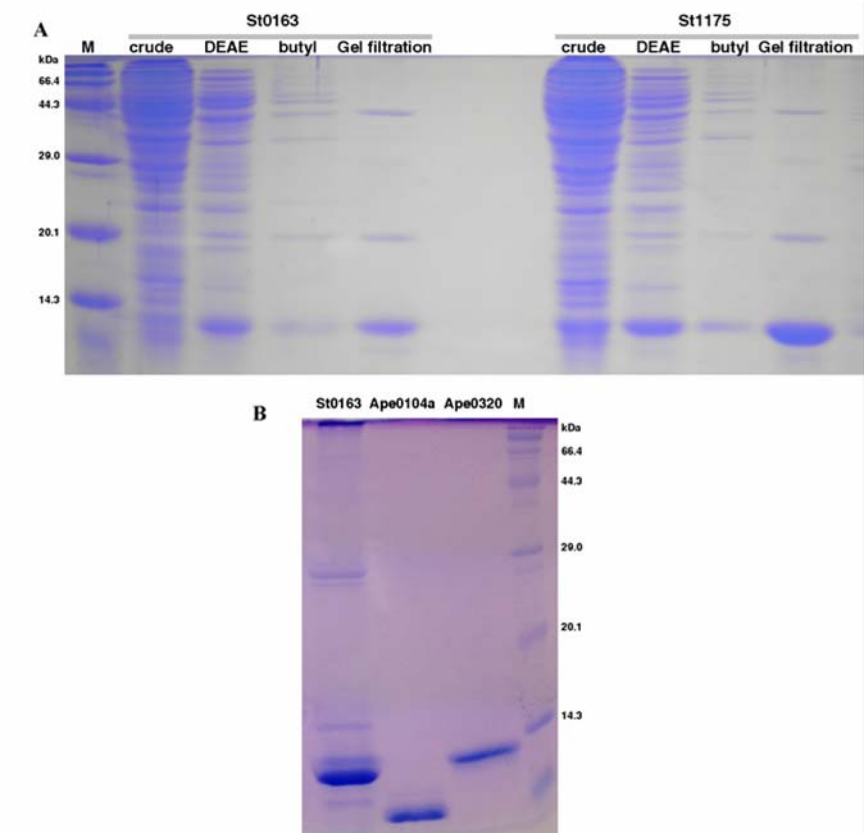

Fig.5-3. SDS-PAGE of various purified recombinant Fds. (A) St0163 and St1175. (B) Ape0320 and Ape0104a

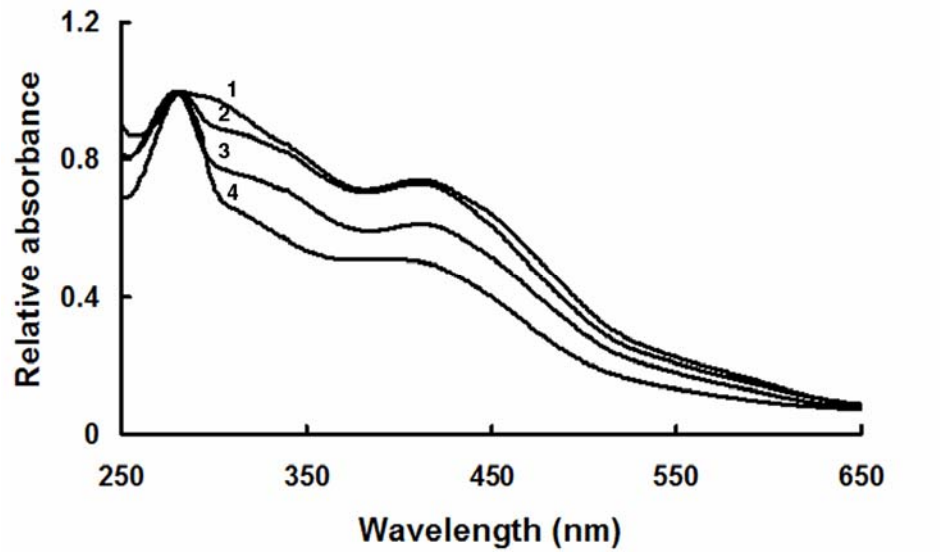

Fig.5-4. Absorption spectra of various recombinant Fds. Relative absorbance was set at A_{280}=1 for each Fd. Traces 1, 2, 3, and 4 stand for the Ape0104a, St0163, St1175, and Ape0320, respectively.

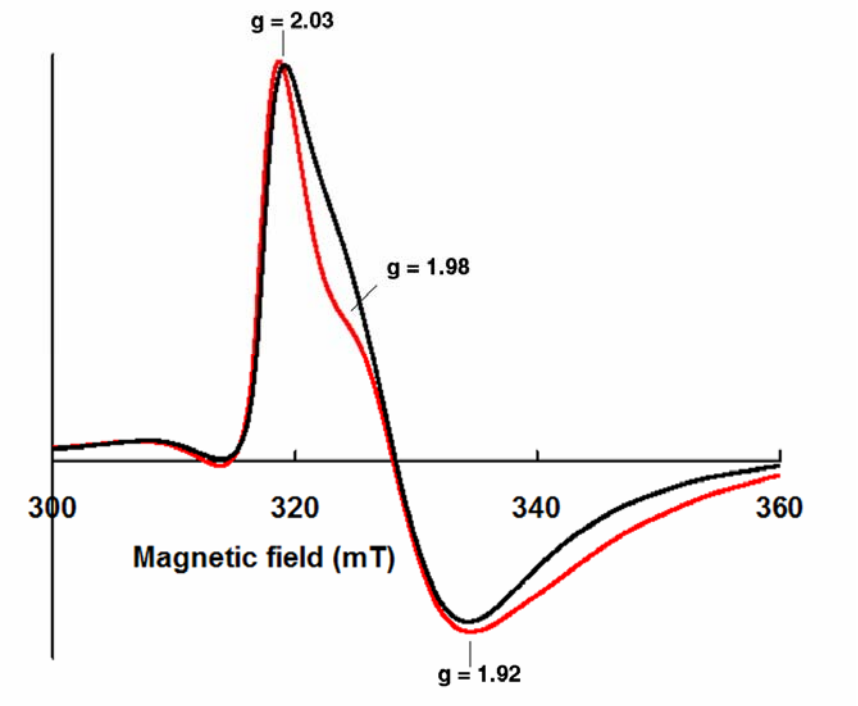

Fig.5-5. EPR spectra of St0163 (red line) and St1175 (black line). EPR spectra were measured at 8K with a microwave power of 1.0 mW and modulation amplitude of 0.8 mT.

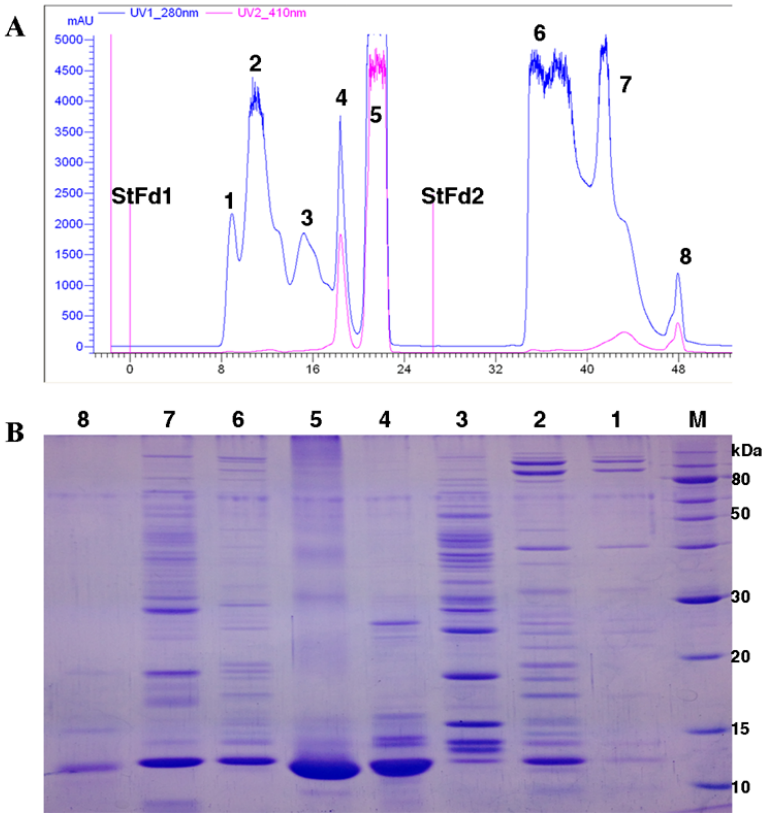

Fig.5-6. Gel filtration (A) and SDS-PAGE (B) of StFd1 and 2 from cytosol of *S. tokodaii*.

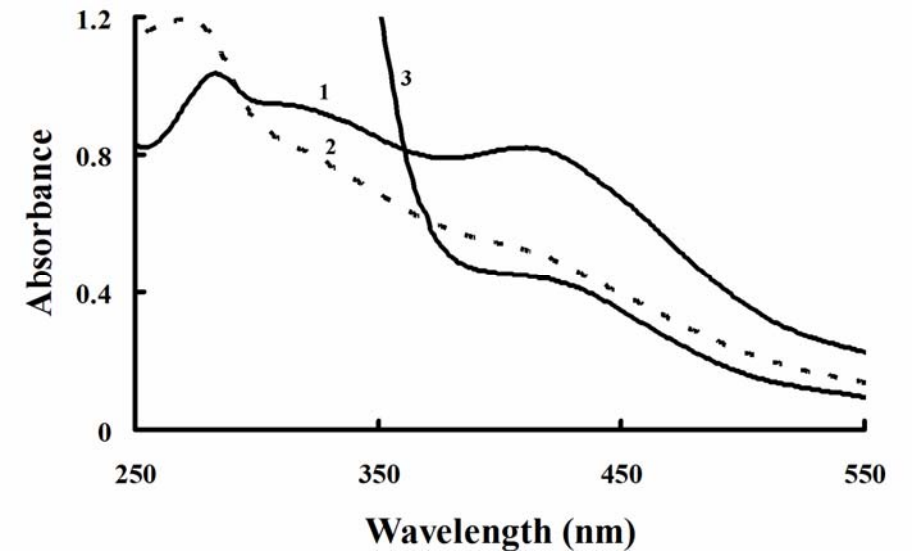

Fig.5-7. Absorption spectra of purified StFd1 and StFd2 from cytosol of *S. tokodaii*. Traces 1, 2, and 3 stand for the StFd1, StFd2, and StFd1 incubated with 10 mM dithionite, respectively.

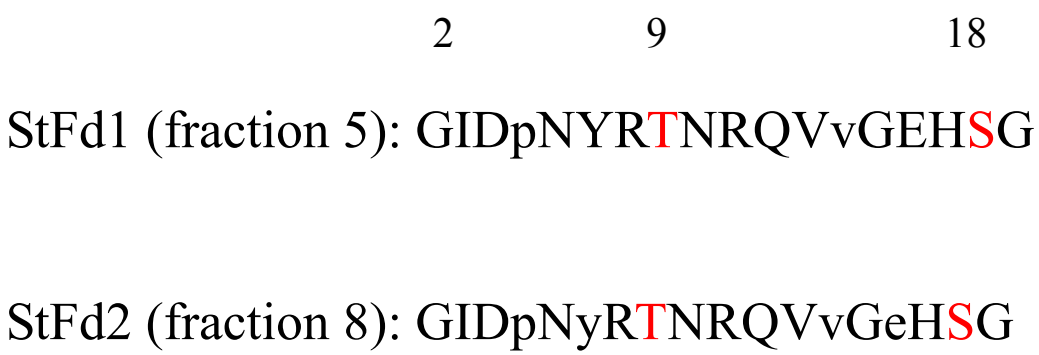

Fig.5-8. Sequence comparison of the N-terminal amino acid sequence of StFd1 and StFd2. Small letters indicate ambiguous residues. Red letters indicate the corresponding residues of difference in St0163 and St1175.

Table 5-1 OFORs activities assayed by various recombinant Fds

U/mg[a]	No Fd	St0163	Ape0104a	Ape0320
StOFOR1	**0.085**	**0.39**	**0.1**	**0.38**
StOFOR2	**0.088**	**0.48**	**0.14**	**0.39**
SsoOFOR	**0.068**	**0.41**	**0.12**	**0.37**
ApeOFOR1	**0.089**	**0.3**	**0.25**	**0.28**

[a]The activities were assayed by observation of reduction of cytochrome *c* at 550 nm, 50℃. 1 U = 1 μmol/mg. See materials and methods for detailed conditions.

Chapter 6 Concluding Remarks

Hyperthermophilic organisms are related to primitive form of life, and their metabolism shows unique aspects such as use of ferredoxin (Fd) as an electron carrier. Their proteins are highly stable but often oxygen-sensitive when iron-sulfur cluster is included. *S. tokodaii* is an aerobic hyperthermophile and contains a large amount of unique Zn-binding Fds. But the metabolic role of Fd is still unclear. This doctor thesis deals mainly with two Fd-dependent enzymes from *S. tokodaii*, 2-oxoacid:Fd oxidoreductase (OFOR) and Fd:$NADP^+$ oxidoreductase (FNR).

In the chapter one, hyperthermophilic archaea was firstly introduced. As the third domain of organism, archaea are clearly distinguishable from the domains of bacteria and eukarya in metabolism routes and catalytic enzymes. Species of *Sulfolobus* and *Aeropyrum*, as two examples of hyperthermophilic archaea, were reviewed in their discovery, unique physiological features and metabolic types. On the other hand, Fd, OFOR and FNR were introduced in detail as the research objects of this work. Their properties, functions and research progress were summarized, and the aim of this work was determined to study the unknown functions and structures of these redox proteins.

In the chapter two, I studied the reaction mechanism of StOFOR through construction of the Cys mutants. Wild type and all the mutants were assayed by UV-visible spectrum, EPR, CD and cyclic voltammetry to determine the state of [4Fe-4S] clusters. A comprehensive analysis of the results showed that all the mutants lost the intact [4Fe-4S] cluster, except the C197A still retained an incomplete one. In addition, activities of oxidative and non-oxidative decarboxylation to yield acetyl-CoA and acetaldehyde, respectively, were also assayed. These results suggest that the intact [4Fe-4S] cluster is necessary to oxidative decarboxylation, but not required for non-oxidative decarboxylation. Remarkably, I found that the non-oxidative decarboxylation is independent on CoA, which is obviously different from a previous report. Finally, I proposed a revised reaction pathway for StOFOR.

In the chapter three, the crystal structure of StOFOR was solved. Through screening several OFORs

of $(ab)_2$ type, I found that the second OFOR existed in *S. tokodaii* (StOFOR2) is more treatable isoform for crystallization, and the structure of $(ab)_2$ type OFOR was successfully determined by StOFOR2. The novel structure consists of two protomers, each of which comprises one a- and b-subunit. Somehow expectedly, TPP is located at the interface between the two subunits derived from different protomers, and the sole [4Fe-4S] cluster is located nearby the surface of b-subunit. Through comparing the pyruvate-binding active site between DaPFOR and StOFOR, I clarified the reasons of broad substrate specificity for StOFOR. The modeled complex structure of StOFOR2 and StFd were manually docked. This is the first crystal structure of $(ab)_2$ type OFOR, and also the first OFOR structure from archaea.

In the chapter four, a new pathway for recycling Fd in *S.tokodaii* was proposed. The putative gene (*st2133*) for FNR was suggested to catalyze the conversion reaction of reduced Fd to oxidized one, and *vice versa*, under aerobic or anaerobic conditions. The FAD-containing enzyme was analyzed by the activities using the combination of NAD(P)H as an electron donor, and various electron donors. At last, the possible role of ST2133 as a member of the redox cycle for ferredoxin is discussed.

In the chapter five, two Fd genes from *S. tokodaii* and two Fd genes from *A. pernix* were heterologously expressed in *E. coli*, and the purified products were characterized. Various recombinant Fds were comparatively analyzed in the state of iron-sulfur cluster and activities for electron acceptors from OFORs. On the other hand, two natural Fds were isolated from cytosol of *S. tokodaii* and sequenced. Results showed that they are the same protein, but differ in the stability of iron-sulfur clusters.

In conclusion, I studied three redox partners from hyperthermophilic archaea. Their functions, structures, and catalytic properties were analyzed by various biochemical and biophysical methods. These works provide a foundation and framework for further study on the redox mechanisms of oxidoreductases.

Referrences

1. Woese, C. R., Sogin, M. L. & Sutton, L. A. (1974) Procaryote phylogeny. I. Concerning the relatedness of Aerobacter aerogenes to Escherichia coli, *J Mol Evol.* **3**, 293-9.
2. Cavicchioli, R. (2011) Archaea--timeline of the third domain, *Nat Rev Microbiol.* **9**, 51-61.
3. Woese, C. R. & Fox, G. E. (1977) Phylogenetic structure of the prokaryotic domain: the primary kingdoms, *Proc Natl Acad Sci U S A.* **74**, 5088-90.
4. Rothschild, L. J. & Mancinelli, R. L. (2001) Life in extreme environments, *Nature.* **409**, 1092-101.
5. Makarova, K. S., Yutin, N., Bell, S. D. & Koonin, E. V. (2010) Evolution of diverse cell division and vesicle formation systems in Archaea, *Nat Rev Microbiol.* **8**, 731-41.
6. Hirata, A., Klein, B. J. & Murakami, K. S. (2008) The X-ray crystal structure of RNA polymerase from Archaea, *Nature.* **451**, 851-4.
7. Cavicchioli, R., Siddiqui, K. S., Andrews, D. & Sowers, K. R. (2002) Low-temperature extremophiles and their applications, *Curr Opin Biotechnol.* **13**, 253-61.
8. Schiraldi, C., Giuliano, M. & De Rosa, M. (2002) Perspectives on biotechnological applications of archaea, *Archaea.* **1**, 75-86.
9. Huber, H., Hohn, M. J., Rachel, R., Fuchs, T., Wimmer, V. C. & Stetter, K. O. (2002) A new phylum of Archaea represented by a nanosized hyperthermophilic symbiont, *Nature.* **417**, 63-7.
10. Stetter, K. O. (2006) Hyperthermophiles in the history of life, *Philos Trans R Soc Lond B Biol Sci.* **361**, 1837-42; discussion 1842-3.
11. Stetter, K. O. (2006) History of discovery of the first hyperthermophiles, *Extremophiles.* **10**, 357-62.
12. Berg, I. A., Kockelkorn, D., Ramos-Vera, W. H., Say, R. F., Zarzycki, J., Hugler, M., Alber, B. E. & Fuchs, G. (2010) Autotrophic carbon fixation in archaea, *Nat Rev Microbiol.* **8**, 447-60.
13. Berg, I. A., Kockelkorn, D., Buckel, W. & Fuchs, G. (2007) A 3-hydroxypropionate/4-hydroxybutyrate autotrophic carbon dioxide assimilation pathway in Archaea, *Science.* **318**, 1782-6.
14. Shivvers, D. W. & Brock, T. D. (1973) Oxidation of elemental sulfur by Sulfolobus acidocaldarius, *J Bacteriol.* **114**, 706-10.
15. Brock, T. D., Brock, K. M., Belly, R. T. & Weiss, R. L. (1972) Sulfolobus: a new genus of sulfur-oxidizing bacteria living at low pH and high temperature, *Arch Mikrobiol.* **84**, 54-68.
16. Siebers, B., Tjaden, B., Michalke, K., Dorr, C., Ahmed, H., Zaparty, M., Gordon, P., Sensen, C. W., Zibat, A., Klenk, H. P., Schuster, S. C. & Hensel, R. (2004) Reconstruction of the central carbohydrate metabolism of Thermoproteus tenax by use of genomic and biochemical data, *J Bacteriol.* **186**, 2179-94.
17. Ahmed, H., Ettema, T. J., Tjaden, B., Geerling, A. C., van der Oost, J. & Siebers, B. (2005) The

semi-phosphorylative Entner-Doudoroff pathway in hyperthermophilic archaea: a re-evaluation, *Biochem J.* **390**, 529-40.
18. Kawarabayasi, Y., Hino, Y., Horikawa, H., Jin-no, K., Takahashi, M., Sekine, M., Baba, S., Ankai, A., Kosugi, H., Hosoyama, A., Fukui, S., Nagai, Y., Nishijima, K., Otsuka, R., Nakazawa, H., Takamiya, M., Kato, Y., Yoshizawa, T., Tanaka, T., Kudoh, Y., Yamazaki, J., Kushida, N., Oguchi, A., Aoki, K., Masuda, S., Yanagii, M., Nishimura, M., Yamagishi, A., Oshima, T. & Kikuchi, H. (2001) Complete genome sequence of an aerobic thermoacidophilic crenarchaeon, Sulfolobus tokodaii strain7, *DNA Res.* **8**, 123-40.
19. Jaubert, C., Danioux, C., Oberto, J., Cortez, D., Bize, A., Krupovic, M., She, Q., Forterre, P., Prangishvili, D. & Sezonov, G. (2013) Genomics and genetics of Sulfolobus islandicus LAL14/1, a model hyperthermophilic archaeon, *Open biology.* **3**, 130010.
20. Albers, S. V., Birkeland, N. K., Driessen, A. J., Gertig, S., Haferkamp, P., Klenk, H. P., Kouril, T., Manica, A., Pham, T. K., Ruoff, P., Schleper, C., Schomburg, D., Sharkey, K. J., Siebers, B., Sierocinski, P., Steuer, R., van der Oost, J., Westerhoff, H. V., Wieloch, P., Wright, P. C. & Zaparty, M. (2009) SulfoSYS (Sulfolobus Systems Biology): towards a silicon cell model for the central carbohydrate metabolism of the archaeon Sulfolobus solfataricus under temperature variation, *Biochem Soc Trans.* **37**, 58-64.
21. Sako, Y., Nomura, N., Uchida, A., Ishida, Y., Morii, H., Koga, Y., Hoaki, T. & Maruyama, T. (1996) Aeropyrum pernix gen. nov., sp. nov., a novel aerobic hyperthermophilic archaeon growing at temperatures up to 100 degrees C, *Int J Syst Bacteriol.* **46**, 1070-7.
22. Kawarabayasi, Y., Hino, Y., Horikawa, H., Yamazaki, S., Haikawa, Y., Jin-no, K., Takahashi, M., Sekine, M., Baba, S., Ankai, A., Kosugi, H., Hosoyama, A., Fukui, S., Nagai, Y., Nishijima, K., Nakazawa, H., Takamiya, M., Masuda, S., Funahashi, T., Tanaka, T., Kudoh, Y., Yamazaki, J., Kushida, N., Oguchi, A., Kikuchi, H. & et al. (1999) Complete genome sequence of an aerobic hyper-thermophilic crenarchaeon, Aeropyrum pernix K1, *DNA Res.* **6**, 83-101, 145-52.
23. Bruschi, M. & Guerlesquin, F. (1988) Structure, function and evolution of bacterial ferredoxins, *FEMS Microbiol Rev.* **4**, 155-75.
24. Knaff, D. B. & Hirasawa, M. (1991) Ferredoxin-dependent chloroplast enzymes, *Biochim Biophys Acta.* **1056**, 93-125.
25. Frolow, F., Harel, M., Sussman, J. L., Mevarech, M. & Shoham, M. (1996) Insights into protein adaptation to a saturated salt environment from the crystal structure of a halophilic 2Fe-2S ferredoxin, *Nat Struct Biol.* **3**, 452-8.
26. Adman, E. T., Sieker, L. C. & Jensen, L. H. (1973) Structure of a bacterial ferredoxin, *J Biol Chem.* **248**, 3987-96.
27. Fujii, T., Hata, Y., Oozeki, M., Moriyama, H., Wakagi, T., Tanaka, N. & Oshima, T. (1997) The crystal structure of zinc-containing ferredoxin from the thermoacidophilic archaeon Sulfolobus sp. strain 7, *Biochemistry.* **36**, 1505-13.
28. Iwasaki, T., Wakagi, T., Isogai, Y., Tanaka, K., Iizuka, T. & Oshima, T. (1994) Functional and evolutionary implications of a [3Fe-4S] cluster of the dicluster-type ferredoxin from the

thermoacidophilic archaeon, Sulfolobus sp. strain 7, *J Biol Chem.* **269**, 29444-50.
29. Kojoh, K., Fukuda, E., Matsuzawa, H. & Wakagi, T. (2002) Zinc-coordination of aspartic acid-76 in Sulfolobus ferredoxin is not required for thermal stability of the molecule, *J Inorg Biochem.* **89**, 69-73.
30. Kojoh, K., Matsuzawa, H. & Wakagi, T. (1999) Zinc and an N-terminal extra stretch of the ferredoxin from a thermoacidophilic archaeon stabilize the molecule at high temperature, *Eur J Biochem.* **264**, 85-91.
31. Kerscher, L. & Oesterhelt, D. (1982) Pyruvate - Ferredoxin Oxidoreductase New Findings on an Ancient Enzyme, *Trends Biochem Sci.* **7**, 371-374.
32. Wieland, O. H. (1983) The mammalian pyruvate dehydrogenase complex: structure and regulation, *Rev Physiol Biochem Pharmacol.* **96**, 123-70.
33. Kerscher, L. & Oesterhelt, D. (1981) The catalytic mechanism of 2-oxoacid:ferredoxin oxidoreductases from Halobacterium halobium. One-electron transfer at two distinct steps of the catalytic cycle, *Eur J Biochem.* **116**, 595-600.
34. Pieulle, L., Guigliarelli, B., Asso, M., Dole, F., Bernadac, A. & Hatchikian, E. C. (1995) Isolation and characterization of the pyruvate-ferredoxin oxidoreductase from the sulfate-reducing bacterium Desulfovibrio africanus, *Biochim Biophys Acta.* **1250**, 49-59.
35. Kerscher, L. & Oesterhelt, D. (1981) Purification and properties of two 2-oxoacid:ferredoxin oxidoreductases from Halobacterium halobium, *Eur J Biochem.* **116**, 587-94.
36. Yun, N. R., Yamamoto, M., Arai, H., Ishii, M. & Igarashi, Y. (2002) A novel five-subunit-type 2-oxoglutalate:ferredoxin oxidoreductases from Hydrogenobacter thermophilus TK-6, *Biochem Biophys Res Commun.* **292**, 280-6.
37. Kunow, J., Linder, D. & Thauer, R. K. (1995) Pyruvate: ferredoxin oxidoreductase from the sulfate-reducing Archaeoglobus fulgidus: molecular composition, catalytic properties, and sequence alignments, *Arch Microbiol.* **163**, 21-8.
38. Hughes, N. J., Clayton, C. L., Chalk, P. A. & Kelly, D. J. (1998) Helicobacter pylori porCDAB and oorDABC genes encode distinct pyruvate:flavodoxin and 2-oxoglutarate:acceptor oxidoreductases which mediate electron transport to NADP, *J Bacteriol.* **180**, 1119-28.
39. Mai, X. & Adams, M. W. (1994) Indolepyruvate ferredoxin oxidoreductase from the hyperthermophilic archaeon Pyrococcus furiosus. A new enzyme involved in peptide fermentation, *J Biol Chem.* **269**, 16726-32.
40. Tersteegen, A., Linder, D., Thauer, R. K. & Hedderich, R. (1997) Structures and functions of four anabolic 2-oxoacid oxidoreductases in Methanobacterium thermoautotrophicum, *Eur J Biochem.* **244**, 862-8.
41. Heider, J., Mai, X. & Adams, M. W. (1996) Characterization of 2-ketoisovalerate ferredoxin oxidoreductase, a new and reversible coenzyme A-dependent enzyme involved in peptide fermentation by hyperthermophilic archaea, *J Bacteriol.* **178**, 780-7.
42. Zhang, Q., Iwasaki, T., Wakagi, T. & Oshima, T. (1996) 2-oxoacid:ferredoxin oxidoreductase from the thermoacidophilic archaeon, Sulfolobus sp. strain 7, *J Biochem.* **120**, 587-99.

43. Siddiqui, M. A., Fujiwara, S. & Imanaka, T. (1997) Indolepyruvate ferredoxin oxidoreductase from Pyrococcus sp. KOD1 possesses a mosaic structure showing features of various oxidoreductases, *Mol Gen Genet.* **254**, 433-9.
44. Arnold, W., Rump, A., Klipp, W., Priefer, U. B. & Puhler, A. (1988) Nucleotide sequence of a 24,206-base-pair DNA fragment carrying the entire nitrogen fixation gene cluster of Klebsiella pneumoniae, *J Mol Biol.* **203**, 715-38.
45. Brostedt, E. & Nordlund, S. (1991) Purification and partial characterization of a pyruvate oxidoreductase from the photosynthetic bacterium Rhodospirillum rubrum grown under nitrogen-fixing conditions, *Biochem J.* **279 (Pt 1)**, 155-8.
46. Kreutzer, R., Dayananda, S. & Klingmuller, W. (1991) Cotranscription of the electron transport protein genes nifJ and nifF in Enterobacter agglomerans 333, *J Bacteriol.* **173**, 3252-6.
47. Williams, K., Lowe, P. N. & Leadlay, P. F. (1987) Purification and characterization of pyruvate: ferredoxin oxidoreductase from the anaerobic protozoon Trichomonas vaginalis, *Biochem J.* **246**, 529-36.
48. Ikeda, T., Ochiai, T., Morita, S., Nishiyama, A., Yamada, E., Arai, H., Ishii, M. & Igarashi, Y. (2006) Anabolic five subunit-type pyruvate:ferredoxin oxidoreductase from Hydrogenobacter thermophilus TK-6, *Biochem Biophys Res Commun.* **340**, 76-82.
49. Ikeda, T., Yamamoto, M., Arai, H., Ohmori, D., Ishii, M. & Igarashi, Y. (2010) Enzymatic and electron paramagnetic resonance studies of anabolic pyruvate synthesis by pyruvate: ferredoxin oxidoreductase from Hydrogenobacter thermophilus, *FEBS J.* **277**, 501-10.
50. Fukuda, E., Kino, H., Matsuzawa, H. & Wakagi, T. (2001) Role of a highly conserved YPITP motif in 2-oxoacid:ferredoxin oxidoreductase: heterologous expression of the gene from Sulfolobus sp.strain 7, and characterization of the recombinant and variant enzymes, *Eur J Biochem.* **268**, 5639-46.
51. Fukuda, E. & Wakagi, T. (2002) Substrate recognition by 2-oxoacid:ferredoxin oxidoreductase from Sulfolobus sp. strain 7, *Biochim Biophys Acta.* **1597**, 74-80.
52. Luo, J., Fukuda, E., Takase, H., Fushinobu, S., Shoun, H. & Wakagi, T. (2009) Identification of the lysine residue responsible for coenzyme A binding in the heterodimeric 2-oxoacid:ferredoxin oxidoreductase from Sulfolobus tokodaii, a thermoacidophilic archaeon, using 4-fluoro-7-nitrobenzofurazan as an affinity label, *Biochim Biophys Acta.* **1794**, 335-40.
53. Carrillo, N. & Ceccarelli, E. A. (2003) Open questions in ferredoxin-NADP+ reductase catalytic mechanism, *Eur J Biochem.* **270**, 1900-15.
54. Arakaki, A. K., Ceccarelli, E. A. & Carrillo, N. (1997) Plant-type ferredoxin-NADP+ reductases: a basal structural framework and a multiplicity of functions, *FASEB J.* **11**, 133-40.
55. Ceccarelli, E. A., Arakaki, A. K., Cortez, N. & Carrillo, N. (2004) Functional plasticity and catalytic efficiency in plant and bacterial ferredoxin-NADP(H) reductases, *Biochim Biophys Acta.* **1698**, 155-65.
56. Aliverti, A., Pandini, V., Pennati, A., de Rosa, M. & Zanetti, G. (2008) Structural and functional diversity of ferredoxin-NADP(+) reductases, *Arch Biochem Biophys.* **474**, 283-91.

57. Seo, D., Kamino, K., Inoue, K. & Sakurai, H. (2004) Purification and characterization of ferredoxin-NADP+ reductase encoded by Bacillus subtilis yumC, *Arch Microbiol.* **182**, 80-9.
58. Ma, K. & Adams, M. W. (2001) Ferredoxin:NADP oxidoreductase from Pyrococcus furiosus, *Methods Enzymol.* **334**, 40-5.
59. Ma, K. & Adams, M. W. (1994) Sulfide dehydrogenase from the hyperthermophilic archaeon Pyrococcus furiosus: a new multifunctional enzyme involved in the reduction of elemental sulfur, *J Bacteriol.* **176**, 6509-17.
60. Chabriere, E., Charon, M. H., Volbeda, A., Pieulle, L., Hatchikian, E. C. & Fontecilla-Camps, J. C. (1999) Crystal structures of the key anaerobic enzyme pyruvate:ferredoxin oxidoreductase, free and in complex with pyruvate, *Nat Struct Biol.* **6**, 182-90.
61. Charon, M. H., Volbeda, A., Chabriere, E., Pieulle, L. & Fontecilla-Camps, J. C. (1999) Structure and electron transfer mechanism of pyruvate:ferredoxin oxidoreductase, *Curr Opin Struct Biol.* **9**, 663-9.
62. Cavazza, C., Contreras-Martel, C., Pieulle, L., Chabriere, E., Hatchikian, E. C. & Fontecilla-Camps, J. C. (2006) Flexibility of thiamine diphosphate revealed by kinetic crystallographic studies of the reaction of pyruvate-ferredoxin oxidoreductase with pyruvate, *Structure.* **14**, 217-24.
63. Mansoorabadi, S. O., Seravalli, J., Furdui, C., Krymov, V., Gerfen, G. J., Begley, T. P., Melnick, J., Ragsdale, S. W. & Reed, G. H. (2006) EPR spectroscopic and computational characterization of the hydroxyethylidene-thiamine pyrophosphate radical intermediate of pyruvate:ferredoxin oxidoreductase, *Biochemistry.* **45**, 7122-31.
64. Ragsdale, S. W. (2003) Pyruvate ferredoxin oxidoreductase and its radical intermediate, *Chem Rev.* **103**, 2333-46.
65. Furdui, C. & Ragsdale, S. W. (2002) The roles of coenzyme A in the pyruvate:ferredoxin oxidoreductase reaction mechanism: rate enhancement of electron transfer from a radical intermediate to an iron-sulfur cluster, *Biochemistry.* **41**, 9921-37.
66. Menon, S. & Ragsdale, S. W. (1997) Mechanism of the Clostridium thermoaceticum pyruvate:ferredoxin oxidoreductase: evidence for the common catalytic intermediacy of the hydroxyethylthiamine pyropyrosphate radical, *Biochemistry.* **36**, 8484-94.
67. Docampo, R., Moreno, S. N. & Mason, R. P. (1987) Free radical intermediates in the reaction of pyruvate:ferredoxin oxidoreductase in Tritrichomonas foetus hydrogenosomes, *J Biol Chem.* **262**, 12417-20.
68. Ma, K., Hutchins, A., Sung, S. J. & Adams, M. W. (1997) Pyruvate ferredoxin oxidoreductase from the hyperthermophilic archaeon, Pyrococcus furiosus, functions as a CoA-dependent pyruvate decarboxylase, *Proc Natl Acad Sci U S A.* **94**, 9608-13.
69. Case, C. L., Rodriguez, J. R. & Mukhopadhyay, B. (2009) Characterization of an NADH oxidase of the flavin-dependent disulfide reductase family from Methanocaldococcus jannaschii, *Microbiology.* **155**, 69-79.
70. Iwasaki, T., Isogai, Y., Iizuka, T. & Oshima, T. (1995) Sulredoxin: a novel iron-sulfur protein of the thermoacidophilic archaeon Sulfolobus sp. strain 7 with a Rieske-type [2Fe-2S] center, *J Bacteriol.*

177, 2576-82.
71. Bock, A. K., Schonheit, P. & Teixeira, M. (1997) The iron-sulfur centers of the pyruvate:ferredoxin oxidoreductase from Methanosarcina barkeri (Fusaro), *FEBS Lett.* **414**, 209-12.
72. Crack, J., Green, J. & Thomson, A. J. (2004) Mechanism of oxygen sensing by the bacterial transcription factor fumarate-nitrate reduction (FNR), *J Biol Chem.* **279**, 9278-86.
73. Uhrigshardt, H., Walden, M., John, H. & Anemuller, S. (2001) Purification and characterization of the first archaeal aconitase from the thermoacidophilic Sulfolobus acidocaldarius, *Eur J Biochem.* **268**, 1760-71.
74. Nemeria, N. S., Chakraborty, S., Balakrishnan, A. & Jordan, F. (2009) Reaction mechanisms of thiamin diphosphate enzymes: defining states of ionization and tautomerization of the cofactor at individual steps, *FEBS J.* **276**, 2432-46.
75. Zhang, B., Crack, J. C., Subramanian, S., Green, J., Thomson, A. J., Le Brun, N. E. & Johnson, M. K. (2012) Reversible cycling between cysteine persulfide-ligated [2Fe-2S] and cysteine-ligated [4Fe-4S] clusters in the FNR regulatory protein, *Proc Natl Acad Sci U S A.* **109**, 15734-9.
76. Przysiecki, C. T., Meyer, T. E. & Cusanovich, M. A. (1985) Circular dichroism and redox properties of high redox potential ferredoxins, *Biochemistry.* **24**, 2542-9.
77. Cammack, R., Rao, K. K., Hall, D. O., Moura, J. J., Xavier, A. V., Bruschi, M., Le Gall, J., Deville, A. & Gayda, J. P. (1977) Spectroscopic studies of the oxidation-reduction properties of three forms of ferredoxin from Desulphovibrio gigas, *Biochim Biophys Acta.* **490**, 311-21.
78. Khoroshilova, N., Popescu, C., Munck, E., Beinert, H. & Kiley, P. J. (1997) Iron-sulfur cluster disassembly in the FNR protein of Escherichia coli by O2: [4Fe-4S] to [2Fe-2S] conversion with loss of biological activity, *Proc Natl Acad Sci U S A.* **94**, 6087-92.
79. Crack, J. C., Green, J., Cheesman, M. R., Le Brun, N. E. & Thomson, A. J. (2007) Superoxide-mediated amplification of the oxygen-induced switch from [4Fe-4S] to [2Fe-2S] clusters in the transcriptional regulator FNR, *Proc Natl Acad Sci U S A.* **104**, 2092-7.
80. Candy, J. M. & Duggleby, R. G. (1998) Structure and properties of pyruvate decarboxylase and site-directed mutagenesis of the Zymomonas mobilis enzyme, *Biochim Biophys Acta.* **1385**, 323-38.
81. Kluger, R. & Tittmann, K. (2008) Thiamin diphosphate catalysis: enzymic and nonenzymic covalent intermediates, *Chem Rev.* **108**, 1797-833.
82. Tittmann, K. (2009) Reaction mechanisms of thiamin diphosphate enzymes: redox reactions, *FEBS J.* **276**, 2454-68.
83. Chabriere, E., Vernede, X., Guigliarelli, B., Charon, M. H., Hatchikian, E. C. & Fontecilla-Camps, J. C. (2001) Crystal structure of the free radical intermediate of pyruvate:ferredoxin oxidoreductase, *Science.* **294**, 2559-63.
84. Nishizawa, Y., Yabuki, T., Fukuda, E. & Wakagi, T. (2005) Gene expression and characterization of two 2-oxoacid:ferredoxin oxidoreductases from Aeropyrum pernix K1, *FEBS Lett.* **579**, 2319-22.
85. Muller, Y. A., Lindqvist, Y., Furey, W., Schulz, G. E., Jordan, F. & Schneider, G. (1993) A thiamin diphosphate binding fold revealed by comparison of the crystal structures of transketolase, pyruvate oxidase and pyruvate decarboxylase, *Structure.* **1**, 95-103.

86. Shaanan, B. & Chipman, D. M. (2009) Reaction mechanisms of thiamin diphosphate enzymes: new insights into the role of a conserved glutamate residue, *FEBS J.* **276**, 2447-53.
87. Wakagi, T., Fujii, T. & Oshima, T. (1996) Molecular cloning, sequencing, and heterologous expression of a novel zinc-containing ferredoxin gene from a thermoacidophilic Archaeon Sulfolobus sp. strain 7, *Biochem Biophys Res Commun.* **225**, 489-93.
88. Ashikawa, Y., Fujimoto, Z., Noguchi, H., Habe, H., Omori, T., Yamane, H. & Nojiri, H. (2006) Electron transfer complex formation between oxygenase and ferredoxin components in Rieske nonheme iron oxygenase system, *Structure.* **14**, 1779-89.
89. Vignais, P. M., Billoud, B. & Meyer, J. (2001) Classification and phylogeny of hydrogenases, *FEMS Microbiol Rev.* **25**, 455-501.
90. Kanai, T., Ito, S. & Imanaka, T. (2003) Characterization of a cytosolic NiFe-hydrogenase from the hyperthermophilic archaeon Thermococcus kodakaraensis KOD1, *J Bacteriol.* **185**, 1705-11.
91. Puchkaev, A. V., Wakagi, T. & Ortiz de Montellano, P. R. (2002) CYP119 plus a Sulfolobus tokodaii strain 7 ferredoxin and 2-oxoacid:ferredoxin oxidoreductase constitute a high-temperature cytochrome P450 catalytic system, *J Am Chem Soc.* **124**, 12682-3.
92. Puchkaev, A. V. & Ortiz de Montellano, P. R. (2005) The Sulfolobus solfataricus electron donor partners of thermophilic CYP119: an unusual non-NAD(P)H-dependent cytochrome P450 system, *Arch Biochem Biophys.* **434**, 169-77.
93. Arcari, P., Masullo, L., Masullo, M., Catanzano, F. & Bocchini, V. (2000) A NAD(P)H oxidase isolated from the archaeon Sulfolobus solfataricus is not homologous with another NADH oxidase present in the same microorganism. Biochemical characterization of the enzyme and cloning of the encoding gene, *J Biol Chem.* **275**, 895-900.
94. Ruocco, M. R., Ruggiero, A., Masullo, L., Arcari, P. & Masullo, M. (2004) A 35 kDa NAD(P)H oxidase previously isolated from the archaeon Sulfolobus solfataricus is instead a thioredoxin reductase, *Biochimie.* **86**, 883-92.
95. Ruggiero, A., Masullo, M., Ruocco, M. R., Grimaldi, P., Lanzotti, M. A., Arcari, P., Zagari, A. & Vitagliano, L. (2009) Structure and stability of a thioredoxin reductase from Sulfolobus solfataricus: a thermostable protein with two functions, *Biochim Biophys Acta.* **1794**, 554-62.
96. Grimaldi, P., Ruocco, M. R., Lanzotti, M. A., Ruggiero, A., Ruggiero, I., Arcari, P., Vitagliano, L. & Masullo, M. (2008) Characterisation of the components of the thioredoxin system in the archaeon Sulfolobus solfataricus, *Extremophiles.* **12**, 553-62.
97. Kobori, H., Ogino, M., Orita, I., Nakamura, S., Imanaka, T. & Fukui, T. (2010) Characterization of NADH oxidase/NADPH polysulfide oxidoreductase and its unexpected participation in oxygen sensitivity in an anaerobic hyperthermophilic archaeon, *J Bacteriol.* **192**, 5192-202.
98. Park, H. J., Reiser, C. O., Kondruweit, S., Erdmann, H., Schmid, R. D. & Sprinzl, M. (1992) Purification and characterization of a NADH oxidase from the thermophile Thermus thermophilus HB8, *Eur J Biochem.* **205**, 881-5.
99. Ward, D. E., Donnelly, C. J., Mullendore, M. E., van der Oost, J., de Vos, W. M. & Crane, E. J., 3rd (2001) The NADH oxidase from Pyrococcus furiosus. Implications for the protection of anaerobic

hyperthermophiles against oxidative stress, *Eur J Biochem.* **268**, 5816-23.
100. Seo, D. & Sakurai, H. (2002) Purification and characterization of ferredoxin-NAD(P)(+) reductase from the green sulfur bacterium Chlorobium tepidum, *Biochim Biophys Acta.* **1597**, 123-32.
101. Ikeda, T., Nakamura, M., Arai, H., Ishii, M. & Igarashi, Y. (2009) Ferredoxin-NADP reductase from the thermophilic hydrogen-oxidizing bacterium, Hydrogenobacter thermophilus TK-6, *FEMS Microbiol Lett.* **297**, 124-30.
102. Gomes, C. M. & Teixeira, M. (1998) The NADH oxidase from the thermoacidophilic archaea Acidianus ambivalens: isolation and physicochemical characterisation, *Biochem Biophys Res Commun.* **243**, 412-5.
103. Muraki, N., Seo, D., Shiba, T., Sakurai, T. & Kurisu, G. (2010) Asymmetric dimeric structure of ferredoxin-NAD(P)+ oxidoreductase from the green sulfur bacterium Chlorobaculum tepidum: implications for binding ferredoxin and NADP+, *J Mol Biol.* **401**, 403-14.
104. Komori, H., Seo, D., Sakurai, T. & Higuchi, Y. (2010) Crystal structure analysis of Bacillus subtilis ferredoxin-NADP(+) oxidoreductase and the structural basis for its substrate selectivity, *Protein Sci.* **19**, 2279-90.
105. Seo, D., Okabe, S., Yanase, M., Kataoka, K. & Sakurai, T. (2009) Studies of interaction of homo-dimeric ferredoxin-NAD(P)+ oxidoreductases of Bacillus subtilis and Rhodopseudomonas palustris, that are closely related to thioredoxin reductases in amino acid sequence, with ferredoxins and pyridine nucleotide coenzymes, *Biochim Biophys Acta.* **1794**, 594-601.
106. Hansen, T., Urbanke, C., Leppanen, V. M., Goldman, A., Brandenburg, K. & Schafer, G. (1999) The extreme thermostable pyrophosphatase from Sulfolobus acidocaldarius: enzymatic and comparative biophysical characterization, *Arch Biochem Biophys.* **363**, 135-47.
107. Zeldovich, K. B., Berezovsky, I. N. & Shakhnovich, E. I. (2007) Protein and DNA sequence determinants of thermophilic adaptation, *PLoS Comput Biol.* **3**, e5.
108. De Vendittis, E., Castellano, I., Cotugno, R., Ruocco, M. R., Raimo, G. & Masullo, M. (2008) Adaptation of model proteins from cold to hot environments involves continuous and small adjustments of average parameters related to amino acid composition, *J Theor Biol.* **250**, 156-71.
109. Snijders, A. P., Walther, J., Peter, S., Kinnman, I., de Vos, M. G., van de Werken, H. J., Brouns, S. J., van der Oost, J. & Wright, P. C. (2006) Reconstruction of central carbon metabolism in Sulfolobus solfataricus using a two-dimensional gel electrophoresis map, stable isotope labelling and DNA microarray analysis, *Proteomics.* **6**, 1518-29.
110. Yeom, J., Jeon, C. O., Madsen, E. L. & Park, W. (2009) Ferredoxin-NADP+ reductase from Pseudomonas putida functions as a ferric reductase, *J Bacteriol.* **191**, 1472-9.
111. Krapp, A. R., Tognetti, V. B., Carrillo, N. & Acevedo, A. (1997) The role of ferredoxin-NADP+ reductase in the concerted cell defense against oxidative damage -- studies using Escherichia coli mutants and cloned plant genes, *Eur J Biochem.* **249**, 556-63.
112. Krapp, A. R., Rodriguez, R. E., Poli, H. O., Paladini, D. H., Palatnik, J. F. & Carrillo, N. (2002) The flavoenzyme ferredoxin (flavodoxin)-NADP(H) reductase modulates NADP(H) homeostasis during the soxRS response of Escherichia coli, *J Bacteriol.* **184**, 1474-80.

113. Sato, Y., Kameya, M., Fushinobu, S., Wakagi, T., Arai, H., Ishii, M. & Igarashi, Y. (2012) A novel enzymatic system against oxidative stress in the thermophilic hydrogen-oxidizing bacterium Hydrogenobacter thermophilus, *PLoS One.* **7**, e34825.
114. Mandai, T., Fujiwara, S. & Imaoka, S. (2009) A novel electron transport system for thermostable CYP175A1 from Thermus thermophilus HB27, *FEBS J.* **276**, 2416-29.
115. Ito, F., Chishiki, H., Fushinobu, S. & Wakagi, T. (2012) Comparative analysis of two glyceraldehyde-3-phosphate dehydrogenases from a thermoacidophilic archaeon, Sulfolobus tokodaii, *FEBS Lett.* **586**, 3097-103.
116. Iwasaki, T., Fujii, T., Wakagi, T. & Oshima, T. (1995) Alternative form of the dicluster ferredoxin from the thermoacidophilic archaeon, Sulfolobus sp. strain 7, *Biochem Biophys Res Commun.* **206**, 563-9.
117. Wakagi, T. & Oshima, T. (1985) Membrane-bound ATPase of a thermoacidophilic archaebacterium, Sulfolobus acidocaldarius, *Biochim Biophys Acta.* **817**, 33-41.

Acknowledgments

I would like to express my sincere gratitude to previous Prof. Takayoshi Wakagi, who accepted, supported and directed my doctor theme. His knowledge, enthusiasm and resourcefulness have been extremely helpful for my research and made it possible for me to successfully complete my doctor study. I also appreciate his care in my life.

I would like to thank my advisor, Prof. Shinya Fushinobu, for his guidance and support during my doctor theme. Prof. Fushinobu taught me with so much knowledge and techniques in the field of X-ray crystal structure, these will play a significant role in my future study life. He also gave me many valuable comments and assistance on my research.

Sincere thanks are also for assitant professor. Takatoshi Arakawa who gave me many instructions and advances benefited me greatly. I thank Dr. Mitsuru Abo for determination of the metal contents.

I thank Mr. Fumiaki Ito and Dr. Im Do-hyun who gave me very great aids especially at the beginning of my study in this lab when the help was instant. I also thank Mr. Shohei Horii, Mr. Tasuku Ito, Mr. Nam Young-woo, Mr. Masayuki Miyake, and Ms Song Hyun-jin who gave me many good advices and help me to solve the problems in my experiments. In addition, I thank the other members of my lab who had made a pleased atmosphere to do research.

As always, I owe my deep gratitude to my family and friends. I am grateful to God for their blessings. Lastly, it is a pleasure to thank all of those who supported me in any respect during my doctor study at the University of Tokyo.